

**MASTER**

**Low-cost End-effector and Controller Design for a Compliant Autonomous Mobile Robot**

de Groot, P.J.M.

*Award date:*  
2018

[Link to publication](#)

**Disclaimer**

This document contains a student thesis (bachelor's or master's), as authored by a student at Eindhoven University of Technology. Student theses are made available in the TU/e repository upon obtaining the required degree. The grade received is not published on the document as presented in the repository. The required complexity or quality of research of student theses may vary by program, and the required minimum study period may vary in duration.

**General rights**

Copyright and moral rights for the publications made accessible in the public portal are retained by the authors and/or other copyright owners and it is a condition of accessing publications that users recognise and abide by the legal requirements associated with these rights.

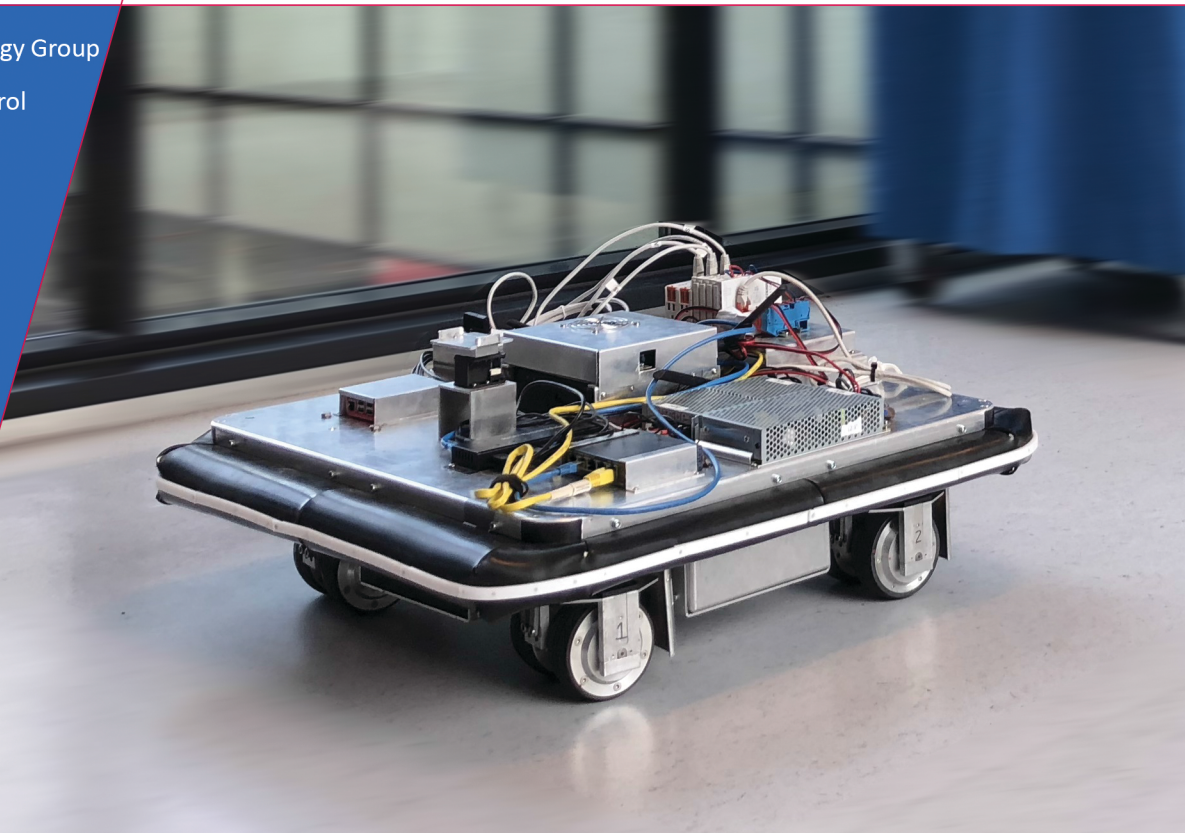
- Users may download and print one copy of any publication from the public portal for the purpose of private study or research.
- You may not further distribute the material or use it for any profit-making activity or commercial gain

/ Department of  
Mechanical Engineering

Control Systems Technology Group

Master Systems and Control

CST 2018.098



# Low-cost End-effector and Controller Design for a Compliant Autonomous Mobile Robot

P.J.M. de Groot  
C.A. López Martínez  
M.J.G. van de Molengraft  
H.P.J. Bruyninckx



## Declaration concerning the TU/e Code of Scientific Conduct for the Master's thesis

I have read the TU/e Code of Scientific Conduct<sup>1</sup>.

I hereby declare that my Master's thesis has been carried out in accordance with the rules of the TU/e Code of Scientific Conduct

Date

24-10-2018

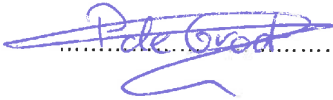
Name

Pieter de Groot

ID-number

0953808

Signature



*Submit the signed declaration to the student administration of your department.*

<sup>1</sup> See: <http://www.tue.nl/en/university/about-the-university/integrity/scientific-integrity/>

The Netherlands Code of Conduct for Academic Practice of the VSNU can be found here also.  
More information about scientific integrity is published on the websites of TU/e and VSNU





# Low-cost End-effector and Controller Design for a Compliant Autonomous Mobile Robot

P.J.M. de Groot, C.A. Lopez Martinez, M.J.G. van de Molengraft and H.P.J. Bruyninckx

**Abstract**—Robots are more often required to work alongside people and should be reliable but most important, safe to use. Especially when the robot directly interacts with a human, the interaction forces must be maintained within safe bounds. In this project, a low-cost passive compliant end-effector is designed as well as a compliant controller. Those are implemented on a mobile robot, such that it is able to deal with interaction forces. A guideline is written on how to choose the end-effector properties such that the safety requirements are met. For experimental purposes, a bumper around the RoPod platform is designed and implemented to be used as end-effector. As a control strategy, Zone-Model Predictive Control (Z-MPC) is proposed. MPC is a control strategy that observes the last state of a process, predict a finite sequence of actions based on a cost function and certain system constraints and executes the first control action. Z-MPC is an addition on standard MPC, replacing the reference by a bounded zone where the states can operate. So Z-MPC minimizes a quadratic cost function in which the minimally required output is calculated to prevent the state from getting outside of the bounded zone. In combination with the bumper system, there is a passive reaction to interaction forces from the bumper and an active one from the controller. The passive reaction is always inherently present, and only when Z-MPC predicts that the interaction forces will get out of bounds, there will be an active reaction as well. With the help of simulations and experiments, the response of the bumper and controller is evaluated and validated in three situations: collision with an object, handling human force interactions and docking to a cart.

**Index Terms**—Mobile Robot, End-effector, Passive Compliance, Interaction Force Control, Model Predictive Control

## I. INTRODUCTION

Nowadays, robotics is rapidly shifting away from an industrial focus and is starting to become more a part of our lives. New robots are designed that can help humans in domains such as healthcare [1], field exploration [2], and cooperative person assistance [3]. In those cases, it is often required that mobile robots are able to move around people, and thus it is becoming inevitable that robots also need to interact, indirect and directly, with humans [4]. The Control Systems Technology (CST) research group from Eindhoven University of Technology (TU/e) is involved in the ROPOD project. The aim of the ROPOD project is to develop an ultra-flat, ultra-flexible, and cost-effective mobile robotic pods for handling legacy in logistics. As a starting point, the focus lies on a mobile robot that is able to support logistics operations in a hospital environment. This robot will execute 24/7 simple tasks such as picking up the laundry or transporting food. The main benefits of a ropod mobile robot for the customers will be a reduction of investment costs for logistics automation,

serves as a force amplifier for the human user and thereby reduces the physical strain on nursing personnel, high quality of services and reputation as hospital using cost-effective, high-end, yet human-friendly technology [5]. When the robot has to operate in an environment with humans, this can pose multiple challenges such as maintaining safety for both the robot as the human, especially with uncertainties in the knowledge of the environment. In terms of safety, conventional robots are made of rigid materials which limit their ability to safely interact with the environment. To account for this, robots should approach mechanical and active compliance and decrease rigidity [6], [7]. The aim of this project is to get a step closer to a safe physical human-robot interaction which opens new possibilities for the use of robots.

### A. Motivation

Robot designers should produce safe products for humans, regardless of which failure, malfunction or mishandle can occur. Therefore, the safety procedures must also be applied to robots [8]. This can be achieved by preventing the robot from getting in contact with a person. The robot and the person can therefore be separated with, for instance, fences or an enclosed space [9]. When it is required for a human to work close to a mobile robot, this is not possible so sensors with the required software are often used to create a safe environment. One of the safety concepts that can be used is based on eliminating contact between the robot and humans or other objects [4]. Because humans can make movements that are not predefined, adaptive robot behaviour is required to prevent physical interaction in those cases. The robot uses sensor outputs to plan trajectories that avoid obstacles and moving objects like, for instance, humans [10]. A disadvantage of such method is that it has difficulties to function in crowded rooms and so it fails to create a safe situation [11]. Also in many cases, a collaboration between worker and robot is required. Therefore, it is not always possible to eliminate contact between the robot and human. Compliant robot behaviour is required to make the robot able to handle the force interactions. A method that can be used is to equip the robot with a force-torque sensor along with force-torque control techniques. Those techniques will restrict robot movements to prevent the maximal interaction force between human and robot is exceeded [12], [13]. The compliant behaviour is achieved through active compliance from the software but it is also possible to achieve this from passive compliance that is built into the manipulator [14]. In that case, the manipulator can be built from non-rigid and

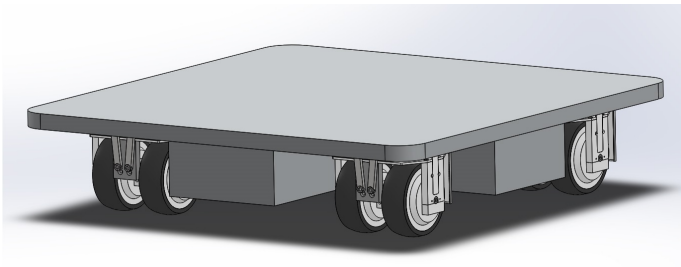


Figure 1: Schematic picture of the Ropod design.

soft material that can adapt passively [15]. In this project, we will combine a soft and compliant end-effector on a mobile robot, with an active compliant controller that will maintain the interaction force within safe bounds. Soft physical interaction with the robot will be possible and the end-effector will provide passive compliance and safety. When forces can not be held within safe bounds with passive compliance, the mobile robot will provide active compliance to maintain safety.

### B. The ropod design

As mobile robot platform for this project, ropod is used. The ropod platform is designed in a square shape as shown in Figure 1 with a low height. By keeping the robot ultra-low, the robot is able to drive under hospital beds and can connect itself by applying a force against the underside of the hospital bed. Another possibility is to connect a cart or load behind the ropod platform. An automated coupling system will be integrated into the platform for the robot to be able to connect to a load autonomously. After connecting, the robot can move the cargo to the desired location. To make it possible for the robot to move, there are differential driven twin wheels mounted near the four corners of the robot. Each individual wheel contains a motor, sensor and motor controller which makes it possible to control each wheel separately. The twin wheels can rotate to any desired direction which makes it possible for the robot to move omnidirectionally. The twin wheels also have a small offset, making them caster wheels. Because of the offset, the wheels rotate when a force is applied to the robot until they are aligned in the direction of the force. This makes it possible to move the robot by hand in an emergency situation when the wheels are not actuated.

### C. Problem statement

The ROPOD project uses as a starting point a hospital environment in where the ropod has to operate autonomously. When robots move around in a hospital environment, situations can occur in which there is a physical interaction between the robot and a human or object. Those situations can cause safety problems. The most common situation is in which the robot has an unexpected collision with an object or a person. This could happen when for example the person makes an unexpected movement or the robot detects the person too



Figure 2: The ropod platform wants to enter the elevator. With the laser, the ropod measures that it will not fit and therefore the ropod will not attempt to enter it. In reality the robot can “squeeze” itself in the elevator and the person will step aside.

late, so a collision cannot be avoided. When the robot makes contact with the object or a person, the interaction force should be within a safe region so the robot’s and the environment’s safety is maintained.

It can also occur that a person directly interacts with the robot because the person wants to move it. This can happen when the robot is driving in a hallway and a person wants to pass the robot with a big object wherefore the robot has to move aside. Here the person in question should be able to push the robot to the desired location and the robot should move along. Also when the robot is standing in front of a door, and people want to open this door from the inside, they should be able to push the robot away with the door. When the person moves the robot away, towards a wall or object, it is possible that the robot may come into contact with that object as well. In such a situation, the robot has to deal with multiple interaction forces that must be maintained within a safe boundary.

Another situation that can occur in a hospital environment is when the robot has to move in a crowded room, like an elevator. In those situations, the robot can have problems with navigation in combination with obstacle avoidance. Standard trajectory tracking navigation ability based on for instance laser data is not sufficient. Figure 2 shows an example situation in which laser data cannot detect a free space in the elevator that meets the size requirements. The robot will therefore not

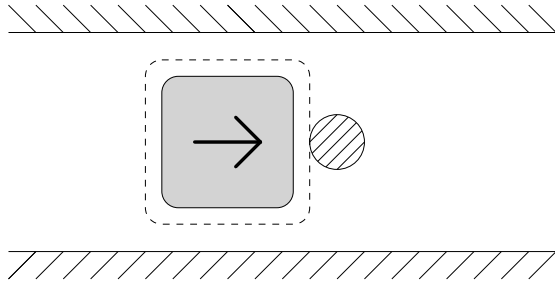


Figure 3: Collision with an object. The interaction force should be maintained within safe bounds.

attempt to enter the elevator. But it can be the case that there is enough space in the elevator only some people are standing in the way. The robot should be able to “squeeze” itself in or out of the elevator. It can then happen that there is a force interaction between the people in the elevator and the robot. The people in the elevator can then make room for the robot. This is acceptable behaviour as long as the interaction force are within safe and pleasant bounds. When the robot is waiting in the elevator, bounded physical contact may occur between a person that is standing alongside the robot. If the physical contact force between the person and robot remains within safe bounds, then the robot does not have to actively respond to this.

#### D. Objectives

In the problem statement of Section I-C, multiple problems have been described that need to be handled correctly by an autonomous mobile robot. Those problems are combined into the main objective that needs to be solved by solving the defined sub-objectives. The main objective is formulated as follows: *Design a low-cost passive compliant end-effector as well as a compliant controller for a mobile robot. The robot should be able to deal with interaction forces while maintaining the robot and its surroundings safe.*

In order to achieve the main objective, it can be divided into the following smaller sub-objectives:

- 1) *End-effector*: Define a guideline and parameter space for an end-effector design that can measure deformations of external forces around the robot and will provide passive compliance of the robot. All the contact between an object and the robot should take place through the end-effector.
- 2) *Collision with an object*: let a mobile robot be able to have an unexpected physical contact (collision) through the end-effector, against an object or human while maintaining the interaction forces within safe bounds as shown in Figure 3. This has to be done with a limited actuation power. In the case of a collision, the interaction force  $F$  should stay below  $F < F_{max}$ . Where  $F_{max}$  is the maximal allowed force according to the ISO norm mentioned in Section I-E to maintain safety.

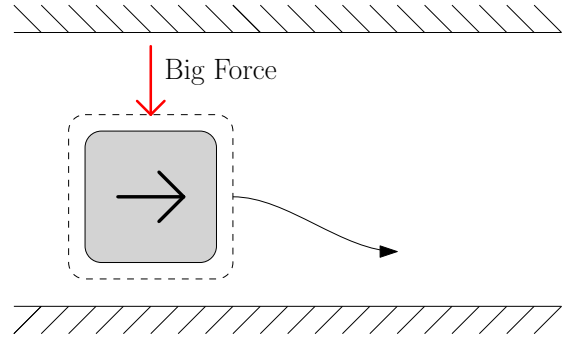


Figure 4: Interaction force from the side. The Robot should not have to react actively on small interaction forces. When the interaction force becomes big, the robot should react on this to maintain safety.

- 3) *Handle multiple interaction forces*: The robot should be able to handle multiple interaction forces and react on those, if necessary, to prevent violating the maximal force limit so a safe situation is maintained as shown in Figure 4. The interaction force  $F$  should stay below  $F < F_{max}$ . Where  $F_{max}$  is the maximal allowed force according to the ISO norm mentioned in Section I-E to maintain safety. The robot does not have to respond actively to small interaction forces that are well below the maximal bound. When the robot has to handle interaction forces in opposite direction, those forces cancel each other out and the robot should only use the resultant force.
- 4) *Dock to a cart*: Make the mobile robot be able to move with a safe speed backward towards a cart and automatically stop after making physical contact with the cart through the end-effector to hold the interaction force  $F$  between  $F_{min} < F < F_{max}$ . The robot should align parallel with the cart so the automatic coupling system can connect the cart. After connecting, the robot will move away with the cart. This situation is shown in Figure 5.  $F_{min}$  is minimal 3N so the robot is able to measure the interaction and  $F_{max}$  is maximal 130N according to the ISO norm mentioned in Section I-E to maintain safety.

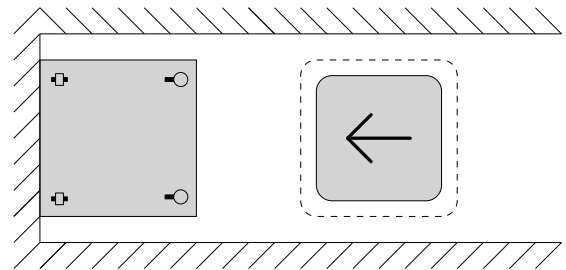


Figure 5: Dock to a cart. There is a minimal interaction force required to hold contact with the cart. The maximal interaction force should be maintained within safe bounds.

### E. Safe interaction

To be able to have a safe interaction between an object or human and the robot, the ISO norm ISO\_TS\_15066 is taken into account. The relevant requirements for this project are:

- Contact situation: Quasi-static contact.
- Body part in contact with the robot: Lower legs.
- Maximum permissible force for the specified body part: 130N.

### F. Outline

This report is divided into five chapters. Chapter I presents the introduction and problem statement. Chapter II presents a guideline on how to make a low cost and passive compliant end-effector. On the basis of this guideline, a prototype has been built for experimental purposes. The design of this prototype, as well as the technical parameters of this bumper, are presented. Chapter III describes how the compliant control is created and which strategy is used to let this controller react as required. Chapter IV contains simulation and experiments of this controller applied to the ropod platform. For the experiments, situations described in the problem statement are tested. Finally, to conclude in Chapter V, the results of those experiments are compared with the desired objectives defined in Chapter I. Possible additions and modifications that can be applied on this project are described in Future work.

## II. BUMPER DESIGN

A passive compliant design of the end-effector is required in the context of robotic interaction, as it improves the safety for both the robot and the environment. To be able to absorb the impact forces, the end-effector should have sufficient damping. This damping should be also limited, otherwise, the interaction force at impact becomes too high. It is desired that the end-effector decompresses after compression and therefore stiffness is required as well. The stiffness is also desired because the deformation of the end-effector is limited. Without stiffness, the distance required for the robot to come to a standstill can become too long. In this chapter, the parameter space of the end-effector is determined. The parameter space contains a combination of stiffness and damping that when applied, should satisfy the safety requirements. A prototype of an end-effector is made on the basis of this parameter space. To check whether the parameters of the prototype fall within the parameter space, the parameters of the end-effector are measured. The prototype will be used later on, in an experiment, to measure if the methods described in this report satisfy the requirements.

### A. Parameter space

The design of the end-effector must satisfy different requirements. A distinction will be made between a forward movement and a sideways movement. In the case of forward

movement, the robot should be able to move with a maximal speed of 1.4m/s. Depending on this speed, the required damping, stiffness and required deformation of the end-effector will be determined. The end-effector is placed around the robot in order to be able to handle interaction forces from different directions. The robot, including the end-effector, may not be wider than a Mobidik (720mm). In this way, the robot fits within the rails where the Mobidiks are stored. With a robot width of 650mm, a maximal allowable extension is 35mm on both sides. Because of this restriction, the maximal speed of a sideways movement will be adjusted to the stiffness, damping and maximum deformation of the end-effector at the sides. For both cases hold that if the robot detects a collision it can brake with a maximal torque of 4Nm/wheel. The robot has 8 wheels with a radius of 52mm, this comes down to a maximum total braking force of  $F_{brk} = 615N$ . To guarantee safety, the parameters of the end-effector will be based on the worst case scenario, where there is a frontal collision with an object. The interaction force should stay below 130N as defined in Chapter I-E.

To calculate the interaction force in the case of a collision, as a function of stiffness and damping of the end-effector, the model of Equation (1) is used.

$$M_r \ddot{x}_r + (b_r + b_c) \dot{x}_r + k_c x_r - F_{brk} \leq F_{max} \quad (1)$$

Where  $M_r$  is the mass of the robot,  $b_c$  is the damping of the cover,  $b_r$  the viscous friction of the robot,  $k_c$  the stiffness of the end-effector,  $x_r$  the deflection of the end-effector,  $F_{brk}$  the breaking power of the robot and  $F_{max}$  the maximal interaction force.

To calculate the maximal damping of the end-effector, we look at the situation where the robot moves constantly at maximal allowed speed and the end-effector makes contact with an object. At the point of impact ( $t = 0s$ ), the acceleration is assumed to be zero, thus, interaction forces at time zero will be a consequence of the initial speed and the damping. With Equation (2), the maximal damping of the cover can be calculated.

$$b_{c_{max}} = \frac{F_{max}}{\dot{x}(0)} \quad (2)$$

For our case, the maximum damping will be 93Ns/m. The possible damping parameters will cover a range from 0 to 93Ns/m. Now the corresponding stiffness range has to be determined from the interaction forces once the collision is detected. We assume that this detection happens immediately as soon as  $x_r > 0$ . The model of Equation (1) will be used to calculate iteratively which stiffness-damping combination satisfies the force and deflection requirements. The model is simulated with different values of  $k_c$  for every  $b_c$ . When the maximal interaction force and maximal deformation do not exceed the constraints, the stiffness and damping parter

combination is taken into account. When doing this for all the stiffness and damping parameters, a design space can be created. Having full breaking power is less crucial when both the interaction force and deflection are far away from the upper constraints, because then there is some room left to come to a standstill and ensure safety. Therefore the parameter combination that has such result are more desirable. To be able to show this in the parameters space, the percentages of how far the maximal force  $F$  and maximal deflection  $x_r$  are away from the bounds are calculated at every stiffness-damping parameter and combined with Equation (3).

$$s(Fn, xn_r) = \sqrt{\frac{Fn^2 + xn_r^2}{F_{max}^2 + xn_{r,max}^2}}$$

$$\text{where : } Fn = \frac{F(k_c, b_c)}{F_{max}}$$

$$xn_r = \frac{x_r(k_c, b_c)}{x_{r,max}}$$
(3)

By combining the force and deflection, we are able to add them to the design space with a colour scale and hold the graph simple without adding multiple dimensions. To be able to combine those values, the values are divided by the maximal constraint to let both the force  $Fn$  and deflection  $xn_r$  have equal weight. The formula for a circle is chosen to combine those values. A small radius of the circle indicates that the deflection and/or force is far away from the maximal constraint. The values of  $s$  are rescaled to a percentages from 0 to 100% where 0% is the point where the interaction force and deflections are the most far away from maximal constraints. Figure 6 shows the design space of an end-effector with a deformation of 60mm. Smaller deformations are possible but the design space will decrease rapidly. When the end-effector has a higher maximal deformation, the design space will grow and the left-bottom corner will be filled. The robot has then more room to come to a standstill with only the breaking power and is less depended on the end-effector.

There are multiple situations in a hospital environment where the robot has to move a load. The maximal speed of the robot needs to be reduced to maintain a safe situation at all times. With the model of Equation (1), a collision is simulated for different initial forward speeds. The maximal allowed speed of which the deformation and interaction forces are within bounds is shown in Figure 7 and indicated with the dotted line. After the robot has determined the weight of the load, it can use this data in the form of, for example, a lookup table, to adjust the maximal allowed forward speed to maintain safety.

### B. Prototype end-effector design

To be able to test if the robot skill of Chapter III works on the ropod platform, a prototype of an end-effector is designed and built. All contact between the moving robot and an object will occur through this end-effector. The designed end-effector should be cost-effective, corresponding to the goal of the ROPOD project. It should also have sufficient

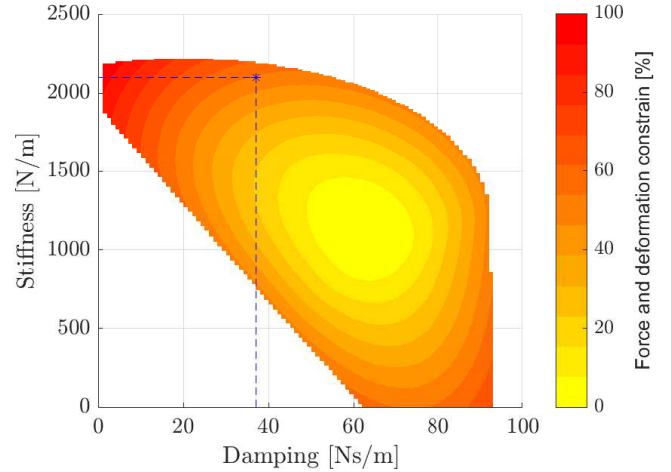


Figure 6: Parameter space of 60mm end-effector. Colors indicate the percentage of how far the force and deformation are from the maximum limit. The dotted line indicates the measured parameters of the implemented bumper.

stiffness and damping as described in Section II-A. To satisfy those requirements, a rubber bumper is chosen as a design for this prototype, made of standard available rubber and lightweight aluminium profiles. The rubber bumper system creates a passive compliant design that is required in the context of robotic interaction. Because it is made of soft material, it provides the safety for both the robot and the environment. A disadvantage of a rubber bumper is that the stiffness is not exactly linear and also not equal at every location as discussed in Section II-C. Using this bumper for experimental purpose will point out further improvements that can be used to design the final end-effector. The bumper is made out of four corner parts so it is easy to handle and install on the ropod platform. The four parts are connected

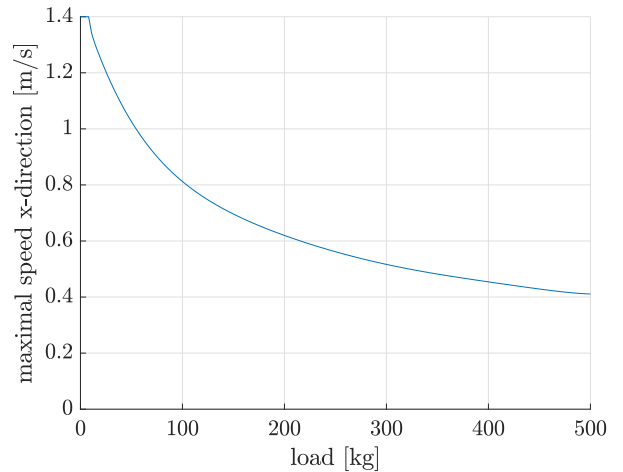


Figure 7: Maximal allowed speed in x-direction depending on the load connected to the robot.





Figure 8: Ropod platform with bumper system.

together for a stiffer connection. The complete design and design choices are described in Appendix A. This bumper is then mounted under the edge of the robot which results in a bumper all around the ropod platform as shown in Figure 8.

Force measurements are required to control the robots movement, this way it is possible to measure if the interaction force stays between bounds. The force measurement is done indirectly by measuring the deformation of the rubber. With an estimation of the stiffness and damping of the rubber, it is possible to calculate the interaction force. Four short-range distance sensors are evenly distributed over each side of the bumper. The distance sensors are read out with an Arduino that is connected to the PC of the robot through USB. The bumper is modeled as four springs and dampers, discretized over the four distance sensors at each side of the bumper as shown in Figure 15. This way the force acting at four parts of the bumper is measured. In order to measure deformation at a point between two sensors, a nylon strip is paced around the outside of the bumper. This relative stiff strip will help to distribute the interaction force evenly over the bumper. It also reduces the friction force between the rubber bumper and an object. The location of the interaction force with respect to the center of the robot is also taken into account. This way the torque applied on the robot can be calculated, which can be used to align with a cart.

For the corner of the bumper, an obtuse angle has been chosen in order to be able to accommodate to small variations such as a hinge when the robot is sliding along a wall. Corners of the rubber bumper are created by cutting the rubber at the fold and then bending the rubber around the corner.

### C. Parameter measurement

To handle interaction forces, the end-effector must be measured to check whether they lie inside the design space shown in Figure 6.

$$k = \frac{F}{x} \quad (4)$$

Hooke's law of Equation (4) is used to determine the stiffness. A load cell is pressed against the bumper and the interaction force with the associated deformation is recorded. The stiffness of the bumper is considered to be linear. The stiffness of the bumper with a thickness of  $35mm$  is  $4489N/m \pm 132N/m$  per sensor, with 95% confidence bounds and the one with the thickness of  $70mm$  is  $1513N/m \pm 24N/m$  per sensor, with 95% confidence bounds. The corners of the bumper are formed by folding the rubber. This results in a higher stiffness at the corners than in the middle part of the bumper. This should be taken into account when the entire bumper is pressed in case the robot connects with a cart or wall. This holds for the bumper of  $70mm$  placed in the x-direction. For this bumper, a stiffness measurement has been done in which a known mass has been placed on the bumper and the associated deflection is measured. In these measurements, the mass is spread over an area of  $200mm$  and the entire bumper. The complete measurement is described in Appendix B-A. Figure 9 show the result of those experiments. This figure shows the stiffness distribution over the length of the bumper. The dotted lines indicate the position of the distance sensors. To deal with the stiffness variation, the measured stiffness in an experiment where a force is exerted against the complete bumper is used in the model of the force controller. This measured average stiffness is  $2068N/m \pm 90N/m$  per sensor with 95% confidence bounds. When using this stiffness, the

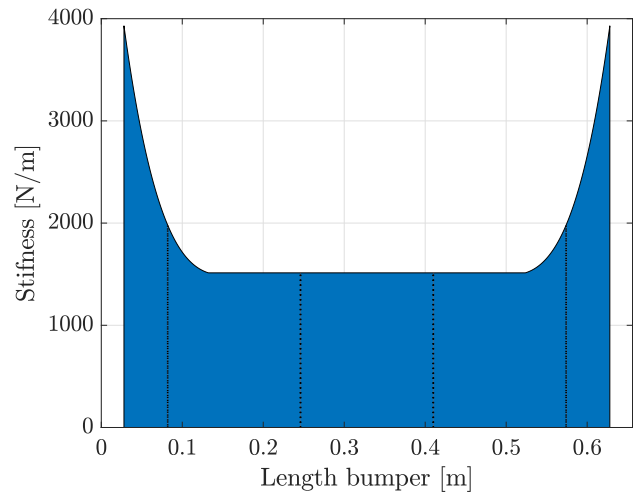


Figure 9: Stiffness variation over the length of the bumper with a thickness of  $70mm$ .



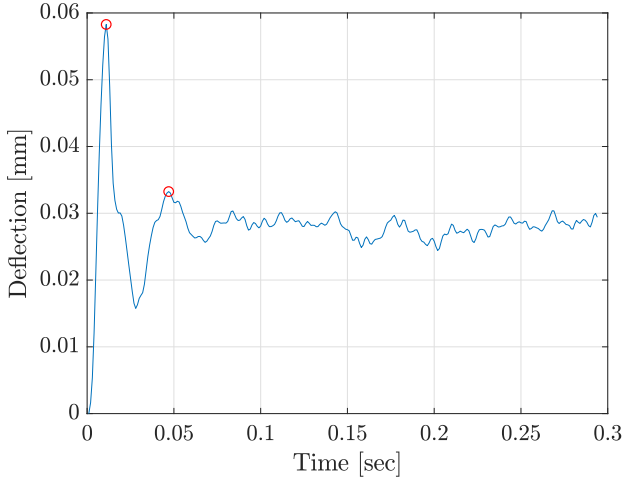


Figure 10: Step response of the bumper with a thickness of 70mm. Used to determine the damping parameter.

total predicted force by the model will correspond to the real measured force in the case of connection with a flat surface and the force controller can react correctly in those situations. When the rod has a collision with a person or object, this will in most cases occur in the middle part of the bumper. The interaction forces will there be estimated higher than they really are. As a result, the response of the force controller will be bigger than really necessary, but the real interaction forces will still remain below the maximal allowed interaction force.

For the damping, the assumption is made that we are dealing with an under-damped system. To determine the damping in the time domain, the logarithmic decrement method is used. An input force is required that results in at least two measurable oscillations. The damping ratio can be calculated from the natural log of the amplitudes of the successive peaks:

$$\delta = \frac{1}{n} \ln \left| \frac{x_1}{x_{n+1}} \right| \quad (5)$$

The damping factor can then be calculated on the basis of this logarithmic decrement by means of:

$$\zeta = \frac{\delta}{\sqrt{4\pi^2 + \delta^2}} \quad (6)$$

After which the damping coefficient can be calculated with:

$$b = 2\zeta \sqrt{\frac{1}{kM}} \quad (7)$$

Where M is the mass of the object causing the oscillation. The mass of the moving part of the bumper is neglected. In the graph of Figure 10, the oscillation of the prototype of the end-effector is shown. A known force is exerted, in the middle of the bumper, at the place of a distance sensor and the deflection

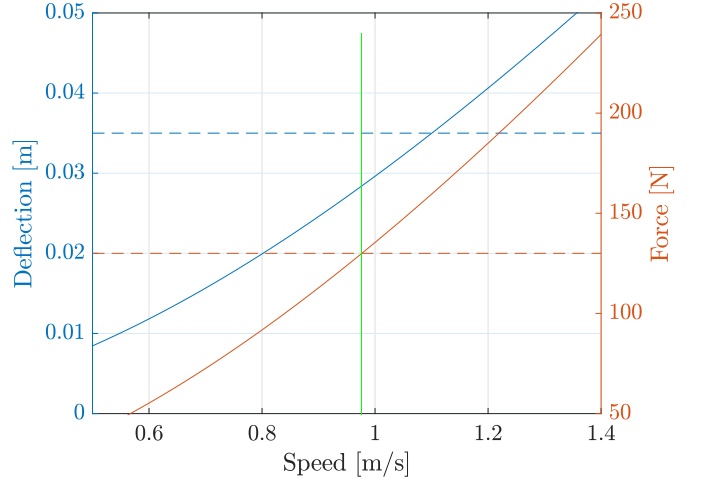


Figure 11: The green line gives the maximal allowed robot speed in y-direction, depending on the interaction force (red) and deflection (blue) in the case of a collision. The dotted lines show the maximally allowed limits.

is measured. The measured damping of the bumper of 70mm is almost the same as of 35mm and falls within the uncertainty. Because of this and for simplicity we assume that the damping is uniform along the bumper. For both thickness's is the damping  $36.6Ns/m \pm 3.9Ns$  with 95% confidence bounds.

The bumper with a thickness of 70mm is placed at the front and back side of the rod. This bumper has a stiffness of approximately  $2100N/m$  and a damping of  $37Ns/m$ . Those values fall within the design space of Figure 6.

The maximal speed of the sideways movement will be determined based on the current prototype of the end-effector. This end-effector has a stiffness of about  $4500N/m$  and a damping of about  $37Ns/m$ . For the sideways movement, the end-effector has a deformation range of 35mm. When those values are simulated, the graph of Figure 11 can be made. To hold the interaction force and deformation below the thresholds, a maximal sideways movement speed of  $0.97m/s$  is allowed.

### III. COMPLIANT CONTROL

The end-effector mounted on the robot creates passive compliance, but this will not always be enough to maintain safety. Therefore compliant control is required to actively react to interactions through the end-effector when the forces become too high to be safe. This force constraint need to be taken into account in the controller. There are multiple controllers that can handle constrains. But because Model Predictive Control (MPC) has also the ability to prevent violating those contains by predicting future states, this controller is chosen for this project. The reference is replaced by a zone and this new controller is called Zone-MPC (Z-MPC). With this zone, the passive reaction from the end-effector is always inherently present, and only when Z-MPC predicts that the interaction

forces will get out of the bounded zone, there will be an active reaction as well. The prediction model, constraint matrices and optimisation problem used for Z-MPC are defined for our situation. In the next chapter, this compliant controller in combination with the bumper is tested on the ropod platform to see if the strategy works as required.

### A. Control strategy

When the interaction forces are measured, the controller must keep the interaction force below the limit  $F_n \leq F_{max}$  to ensure safety. In the case where the robot has to connect to a flat surface and hold contact, also a minimal interaction force is required,  $F_n \geq F_{min}$ . Within those constraints, the size of the interaction force is not important. So there exists a constraint zone  $F_{min} \leq F_n \leq F_{max}$  in where the robot is allowed to operate. The power of the motors that actuate the robot and the deflection of the bumper are also limited and needs to be taken into account.

In simple feedback controllers, as for example PID, a reference tracking controller observes the last state of a process, measures the error, calculates a new input and implement the control action [16]. Simple feedback controllers do not incorporate constraints. Because the force constraint is important in this project, those controllers cannot be used. Examples of controllers that can handle constraints and a constrained zone are: Fuzzy logic, Quadratic Dynamic Matrix Control, Sliding Mode Control and Zone Model Predictive Control (Z-MPC). Fuzzy logic is a form of many-valued logic in which the truth values of variables may be any real number between 0 and 1. Fuzzy logic is all about the relative importance of precision and has the ability to deal with imprecise and vague information [17]. Quadratic Dynamic Matrix Control is a multi variable algorithm which provides a direct and efficient method for handling process constraints [18]. Sliding mode control implies that control actions are discontinuous state functions which may easily be implemented by conventional power converters with on-off as the only admissible operation mode [19]. Model Predictive Control (MPC) is a predictive controller, that observes the last state of a process, predict a finite sequence of actions and implement the first input. Thus, MPC offers the feature of “Looking Ahead” while coping with constraints. The reference can be removed and replace by a zone, bounded by force constraints [20]. For the choice of the controller we have looked at the main design factor, namely safety. It is undesirable to wait until the error crosses the maximal force constraint before acting because this increases the chances of harming the environment and the robot itself. Because of the possibility to prevent violation of the force constraints by predicting the future states and reacting on forehand, Z-MPC is chosen as control strategy. This outweigh the higher implementation effort because of the complexity of Z-MPC in comparison with the other controllers. Z-MPC uses a cost function to calculate the minimal output to hold the states within the constrained zone. This has as benefit that

unnecessary control actions are prevented and energy saved. So when a human interacts with the end-effector, there is a passive reaction to the interaction force from the bumper. Only when Z-MPC predicts that the interaction forces will get out of the constrained zone, there will be an active reaction from the controller as well. It is even possible to change the constraints online, which makes it is possible to let the controller react differently in different situations described in Section I-C. In combination with the bumper system, this creates the possibility for safe robot-human interaction.

MPC has the ability to handle constraints. Constraints are present in this system on the input  $u$  and on the output interaction force  $F_d$  and deflection  $x_l$ . The constraints on the input are fixed, the motor of the robot cannot deliver more power than its maximum power. This also applies to deflection, the bumper can only deflect for a defined amount. The constraints on the interaction forces are different. Those can be exceeded when an unexpectedly large disturbance has occurred, so there is really no way in which the system can be kept within the specified constraints. A serious problem can occur with the predictive control problem, because the optimizer may be faced with an infeasible problem. A straightforward way to solve this problem is by softening the output constraints. This can be done by adding a new variable  $\epsilon$ , the so-called “slack variable”, which is defined in such a way that it is non-zero only if the constraints are violated [20]. What should be taken into account is that adding soft constraints has consequences for the computation time of the controller. To minimize this effect, only one slack variable is introduced as described in Section III-E. This helps to hold computation time below ( $< 0.01sec$ ) to prevent under-sampling. Another reason why only one soft constraint has been used is to prevent conflicts between soft constraints. With one soft constraint it is clear what the goal of the optimization problem is, namely to get this constraint back within the bounds. With multiple soft constraints, the controller has to calculate which constraint it first has to get within the bounds. This can cause undesirable behaviour where the other soft constraint may be exceeded further.



Figure 12: Z-MPC with soft constraints. The state of the system can move freely within the constrained zone. When a constraint is violated, this is very heavily penalized so maximal possible control action is used to get within constraints again.

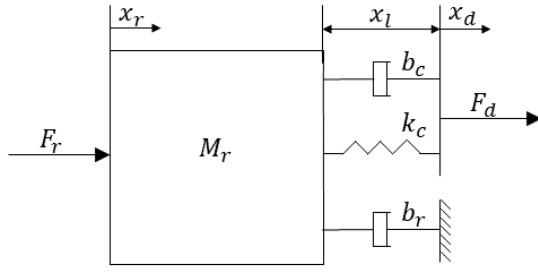


Figure 13: Simplified system representation  $x$ -direction.

Figure 12 gives a schematic representation of the expected result of Z-MPC with soft constraints. The blue line gives the state of the system that is within bounds at this time step. But Z-MPC predicts that with the current disturbance, it is not possible to prevent violating the constraints in the future. This violation is very heavily penalized so the maximal possible control action is used to get the system within bounds as fast as possible.

### B. Dynamical plant model

MPC uses a model of the system to predict the behavior of the system in the future. For this purpose a simplified representation of the system is made as shown in Figure 13. For this project, it is assumed that  $x$ - and  $y$ -movement of the robot is decoupled because the robot is omni directional as described in Section I-B. So a separated controller is created for both  $x$ - and  $y$ -direction. The controllers are built up the same only the parameters differ.

The robot can be represented as a mass with friction and the end-effector as a spring and damper as shown in Figure 13. Therefore the dynamical model of the system can be written as:

$$M_r \ddot{x}_r + (b_r + b_c) \dot{x}_r + k_c x_r = F_r + \underbrace{b_c \dot{x}_d + k_c x_d}_{F_d} \quad (8)$$

Where  $M_r$  is the mass of the robot,  $b_r$  the viscous friction of the robot,  $b_c$  the damping of the end-effector,  $k_c$  the stiffness of the end-effector,  $F_r$  the controlled robot force and  $F_d$  the disturbance force as for example the interaction force from a human hand. This model is used as a prediction model to predict the interaction force from the current state. Therefore we should be able to get the amount  $x_l$ , and speed  $\dot{x}_l$ , of the deflection from this model. With the estimated stiffness and damping of the end-effector, the interaction force can then be calculated. To get the amount and the speed of the deflection, the state of the disturbance need to be subtracted from the state of the robot ( $x_l = x_r - x_d$  and  $\dot{x}_l = \dot{x}_r - \dot{x}_d$ ). Now the state of the end-effector is represented in the equation, so it is possible to put constraints on those states later on, to limit the interaction force.

$$M_r \ddot{x}_r + b_r \dot{x}_r + b_c (\underbrace{\dot{x}_r - \dot{x}_d}_{\dot{x}_l}) + k_c (\underbrace{x_r - x_d}_{x_l}) = F_r \quad (9)$$

This dynamical model can be written in state space representation of Equation (10). Matrix  $A$ ,  $B$ , and  $B_d$  are based on the model from Equation (9). The matrix  $A_d$  contains the disturbance model. We assume that the current disturbance speed is also the speed in the next time step unless the robot reacts on this. Therefore the speed of the disturbance is included in the disturbance model. This is chosen so that when the robot, for example, has a collision with an object, the impact speed is used to calculate whether the interaction force becomes too high in the future. Matrix  $C$  and  $C_d$  give the system output, which is the deflection  $x_l$  and deflection speed  $\dot{x}_l$  of the end-effector.

$$\begin{aligned} \begin{bmatrix} \dot{x}_r \\ \ddot{x}_r \end{bmatrix} &= \underbrace{\begin{bmatrix} 0 & 1 \\ \frac{-k_c}{M_r} & \frac{-(b_r+b_c)}{M_r} \end{bmatrix}}_A \begin{bmatrix} x_r \\ \dot{x}_r \end{bmatrix} + \underbrace{\begin{bmatrix} 0 \\ \frac{1}{M_r} \end{bmatrix}}_B [F_r] + \underbrace{\begin{bmatrix} 0 & 0 \\ \frac{k_c}{M_r} & \frac{b_c}{M_r} \end{bmatrix}}_{B_d} \begin{bmatrix} x_d \\ \dot{x}_d \end{bmatrix} \\ \begin{bmatrix} \dot{x}_d \\ \ddot{x}_d \end{bmatrix} &= \underbrace{\begin{bmatrix} 0 & 1 \\ 0 & 0 \end{bmatrix}}_{A_d} \begin{bmatrix} x_d \\ \dot{x}_d \end{bmatrix} \\ \begin{bmatrix} x_l \\ \dot{x}_l \end{bmatrix} &= \underbrace{\begin{bmatrix} 1 & 0 \\ 0 & 1 \end{bmatrix}}_C \begin{bmatrix} x_r \\ \dot{x}_r \end{bmatrix} + \underbrace{\begin{bmatrix} -1 & 0 \\ 0 & -1 \end{bmatrix}}_{C_d} \begin{bmatrix} x_d \\ \dot{x}_d \end{bmatrix} \end{aligned} \quad (10)$$

The matrices  $A$ ,  $A_d$ ,  $B$ ,  $B_d$ ,  $C$  and  $C_d$  of Equation (10) are combined to get one state space representation of the system. For simplicity the states are denoted as  $X = [x_r \quad \dot{x}_r \quad x_d \quad \dot{x}_d]^\top$ , the input as  $u = F_r$  and the output as  $Y = [x_l \quad \dot{x}_l]^\top$ . The combined system can be written as:

$$\begin{aligned} \dot{X} &= \underbrace{\begin{bmatrix} A & B_d \\ 0 & A_d \end{bmatrix}}_A X + \underbrace{\begin{bmatrix} B \\ 0 \end{bmatrix}}_B u \\ Y &= \underbrace{\begin{bmatrix} C & C_d \end{bmatrix}}_C X \end{aligned} \quad (11)$$

The model of Equation (11) is discretized with the Zero-order hold method. This results in new  $A$ ,  $B$  and  $C$  matrices representing the discretized system including disturbance model.

### C. Prediction model

To be able to predict the future state of the system, MPC uses prediction Equation (12) [20]. The prediction equation is formulated as follows:

$$\begin{bmatrix} X_{1|k} \\ X_{2|k} \\ \vdots \\ X_{N|k} \end{bmatrix} = \underbrace{\begin{bmatrix} A \\ A^2 \\ \vdots \\ A^N \end{bmatrix}}_{\Phi} X_{0|k} + \underbrace{\begin{bmatrix} B & 0 & \cdots & 0 \\ AB & B & \cdots & 0 \\ \vdots & \vdots & \ddots & \vdots \\ A^{N-1} & A^{N-2} & \cdots & B \end{bmatrix}}_{\Gamma} \begin{bmatrix} u_{0|k} \\ u_{1|k} \\ \vdots \\ u_{N-1|k} \end{bmatrix} \quad (12)$$

Where  $X_k$  and  $u_k$  are the predicted states and inputs respectively,  $\Phi$  and  $\Gamma$  are the prediction matrices and  $N$  the prediction horizon. When written in the compact form, Equation (13) remains.

$$X_k^* = \Phi X_k + \Gamma U_k \quad (13)$$

#### D. Constraints

In this section, the constraints are defined. For the first constraint, the motor power is taken into account. The motor of the robot cannot deliver more power than its maximum power so the input has a hard constraint:

$$F_r^{low} \leq u_{i|k} \leq F_r^{high}, \quad \forall i = 0, 1, \dots, N-1 \quad (14)$$

For this project, the interaction force must be constrained to maintain safety in the case of human-robot interaction. The interaction force can be calculated by  $b_c(\dot{x}_{c_{i|k}} - \dot{x}_{d_{i|k}}) + k_c(x_{c_{i|k}} - x_{d_{i|k}})$  where  $\dot{x}_{c_{i|k}} - \dot{x}_{d_{i|k}}$  can be denoted as  $\dot{x}_{l_{i|k}}$  and  $x_{c_{i|k}} - x_{d_{i|k}}$  as  $x_{l_{i|k}}$ . The interaction force is bounded by the minimal and maximal force constraints. To make those constraints soft as described in Section III-A, the variable  $\epsilon$  is added.

$$F_d^{low} - \epsilon \leq b_c \dot{x}_{l_{i|k}} + k_c x_{l_{i|k}} \leq F_d^{high} + \epsilon, \quad \forall i = 1, 2, \dots, N \quad (15)$$

$\epsilon \geq 0, \quad \forall i = 1, 2, \dots, N$

When the bumper is deflected at a low speed, it is possible to completely deflect the bumper without violating the force constraints. Because the deflection of the bumper is physically bounded, this is added to the constraints and set as a hard constraint.

$$x_l^{low} \leq x_{l_{i|k}} \leq x_l^{high}, \quad \forall i = 1, 2, \dots, N \quad (16)$$

The constraints can be equivalently written as:

$$\underbrace{\begin{bmatrix} 0 & 0 & 0 & 0 \\ 0 & 0 & 0 & 0 \\ k_c & b_c & -k_c & -b_c \\ 1 & 0 & -1 & 0 \\ -k_c & -b_c & k_c & b_c \\ -1 & 0 & 1 & 0 \end{bmatrix}}_{M_i} X_{i+1|k} + \underbrace{\begin{bmatrix} -1 \\ 1 \\ 0 \\ 0 \\ 0 \\ 0 \end{bmatrix}}_{E_i} u_{i|k} \leq \underbrace{\begin{bmatrix} F_r^{high} \\ -F_r^{low} \\ F_d^{high} \\ x_l^{high} \\ -F_d^{low} \\ -x_l^{low} \end{bmatrix}}_{b_i} + \underbrace{\begin{bmatrix} 0 \\ 0 \\ 1 \\ 1 \\ 0 \\ 0 \end{bmatrix}}_{h_i} \epsilon, \quad (17)$$

$\forall i = 0, 1, \dots, N-1$

$$\underbrace{\begin{bmatrix} k_c & b_c & -k_c & -b_c \\ 1 & 0 & -1 & 0 \\ -k_c & -b_c & k_c & b_c \\ -1 & 0 & 1 & 0 \end{bmatrix}}_{M_n} X_{i+1|k} \leq \underbrace{\begin{bmatrix} F_d^{high} \\ x_l^{high} \\ -F_d^{low} \\ -x_l^{low} \end{bmatrix}}_{b_N} + \underbrace{\begin{bmatrix} 1 \\ 0 \\ 1 \\ 0 \end{bmatrix}}_{h_N} \epsilon \quad (18)$$

Grouping all the constraints together yields:

$$\underbrace{\begin{bmatrix} M_0 \\ 0 \\ \vdots \\ 0 \end{bmatrix}}_D X_{0|k} + \underbrace{\begin{bmatrix} 0 & \cdots & 0 \\ M_1 & \cdots & 0 \\ \vdots & \ddots & \vdots \\ 0 & \cdots & M_N \end{bmatrix}}_M \begin{bmatrix} X_{1|k} \\ \vdots \\ X_{N|k} \end{bmatrix} + \underbrace{\begin{bmatrix} E_0 & \cdots & 0 \\ \vdots & \ddots & \vdots \\ 0 & \cdots & E_{N-1} \\ 0 & \cdots & 0 \end{bmatrix}}_E \begin{bmatrix} u_{0|k} \\ \vdots \\ u_{N-1|k} \end{bmatrix} \leq \underbrace{\begin{bmatrix} b_0 \\ b_1 \\ \vdots \\ b_N \end{bmatrix}}_c + \underbrace{\begin{bmatrix} r_0 \\ r_1 \\ \vdots \\ r_N \end{bmatrix}}_H \epsilon_k \quad (19)$$

When written in the compact form, Equation (20) remains.

$$DX_k + MX_k^* + EU_k \leq c + H\epsilon_k \quad (20)$$

After substituting the prediction model of Equation (13) into the constraint Equation (20), results in:

$$GU_k \leq c + WX_k + H\epsilon_k \quad (21)$$

where  $G = M\Gamma + E$   
 $W = -D - M\Phi$

The condition  $\epsilon \geq 0$  is added to Equation (21) and  $\epsilon$  is combined with  $U_k$  to simplify the equation:

$$\underbrace{\begin{bmatrix} g_{1,1} & \cdots & g_{1,N} & -r_0 \\ \vdots & \ddots & \vdots & \vdots \\ g_{N,1} & \cdots & g_{N,N} & -r_N \\ 0 & \cdots & 0 & -1 \end{bmatrix}}_L \underbrace{\begin{bmatrix} u_{0|k} \\ \vdots \\ u_{N-1|k} \\ \epsilon_k \end{bmatrix}}_{U_k^*} \leq c + WX_k \quad (22)$$

This results in:

$$LU_k^* \leq c + WX_k \quad (23)$$

#### E. MPC cost function

In Equation (24) [20] the standard cost function of MPC is shown.

$$J(x(k), U_k) = x_{N|k}^\top P x_{N|k} + \sum_{i=0}^{N-1} (x_{i|k}^\top Q x_{i|k} + u_{i|k}^\top R u_{i|k}) \quad (24)$$

To be able to use Z-MPC, no reference trajectory is used and the state penalty  $Q$ , as well as terminal cost weight  $P$ , is set to

zero. This is done because in our case it is not important what the state of the system is, as long as it is within the constraints. What is interesting, is the minimum required input to stay within the constraints. This way unnecessary control actions are prevented and battery power can be saved. Soft constraints are taken into account so the cost function becomes:

$$J(U_k, \epsilon_k) = \sum_{i=0}^{N-1} \left( u_{i|k}^\top R u_{i|k} + \rho \max_i \epsilon_{i|k} \right) \quad (25)$$

The soft constraints are added by the slack variable  $\epsilon$  and very heavily penalized by  $\rho$  in the cost function as shown in Equation (25). To implement  $\rho$  in the cost function, a quadratic penalty can be used. The optimizer will have a strong incentive to keep  $\epsilon$  at zero if possible. This method has a drawback, because when the constrain is active, all finite values of  $\rho$  will result in them being violated to some extent, even if this is not necessary. To solve this problem,  $\rho$  can be implemented as  $1 - norm$  or  $\infty - norm$ . The  $\infty - norm$  is more efficient and therefore chosen for this project. With this method, only one slack variable is introduced, which gives, in general, a much faster algorithm [20]. The exact value of  $\rho$  has to be defined. If  $\rho = 0$ , the constraint is not taken into account, and if  $\rho = \infty$ , the constraint is a hard constraint [20]. When using the  $\infty - norm$ , the soft constrain will be defined in the cost function as  $\rho\epsilon$ . Together with the output  $Ru^2$ , those are minimised while still satisfying the constrains. In the case constraints are approached, the maximal power should be used to get the system within constraints. When using  $u_{max}$  is not enough to satisfies the constraints, the soft constraint should be used. Therefore  $\rho$  has to be chosen to be  $\rho \geq Ru_{max}^2$ .

The parameter  $P$  is normally used to ensure that the final state of the system is stable by using the outcome of the Riccati equation as  $P$  in unconstrained cases. Because of the use of the disturbance model the system is not controllable and so the Riccati equation has no solution, therefore the system is stable within the constraints as long as infinite high disturbances are prevented. Now the only weighting parameter is  $R$ , but because the ratio between  $R$  and  $\rho$  is constant, changing  $R$  will have no influence and therefore set to 1. The MPC cost function can be written as:

We can write out  $J$  from Equation (25) as a function of  $U_k$  and  $\epsilon_k$ , where  $\epsilon$  is written as a scalar because of the use of the  $\infty - norm$ .

$$J(U_k, \epsilon_k) = \underbrace{\begin{bmatrix} u_{0|k} \\ u_{1|k} \\ \vdots \\ u_{N-1|k} \end{bmatrix}}_{U_k} \underbrace{\begin{bmatrix} R & & & \\ & R & & \\ & & \ddots & \\ & & & R \end{bmatrix}}_{\Psi} \underbrace{\begin{bmatrix} u_{0|k} \\ u_{1|k} \\ \vdots \\ u_{N-1|k} \end{bmatrix}}_{U_k} + \underbrace{\begin{bmatrix} \rho & & & \\ & \rho & & \\ & & \ddots & \\ & & & \rho \end{bmatrix}}_{\Omega} \epsilon_k \quad (26)$$

To be able to implement this cost function, the cost function is rewritten as:

$$J(U_k, \epsilon_k) = U_k^\top \Psi U_k + \Omega \epsilon_k \quad (27)$$

#### F. Constrained optimization

Combining the Z-MPC cost function of Equation (27) and the constraints Equation (23) results in Equation (28) that need to be solved to calculate the control input.

$$J(U_k, \epsilon_k) = U_k^\top \Psi U_k + \Omega \epsilon_k \rightarrow \min_{U_k, \epsilon_k} \quad (28)$$

*subject to* :  $LU_k^* \leq c + WX_k$

Equation (28) is a Quadratic Program (QP) that can be solved with a QP solver subject to the constraint equation. The soft constraint parameter  $\epsilon$  is included in the vector  $c$  as described in Section III-D.

$$U_k^* = \arg \min_{U_k, \epsilon_k} U_k^\top \Psi U_k + \Omega \epsilon_k \quad (29)$$

*subject to* :  $LU_k^* \leq c + WX_k$

After solving the QP problem, the first optimal control input can be applied to the plant:

$$u_{MPC} = u_{0|k}^* = [1 \quad 0 \quad \cdots \quad 0] U_k^* \quad (30)$$

## IV. RESULTS

To test the compliant control strategy from Chapter III, a force interaction is simulated that must be hold within constraints. For a realistic result that is comparable with the actual situation, the parameters of the ropod platform are determined and used in this simulation. Also, the numerical values of the controller parameters are defined. After positive results from the simulations, the control strategy is implemented on the ropod platform. Because relatively cheap sensors are used, the signal must first be processed before it can be used to calculate the desired control output. For the robot to work in different situations, a control strategy is made based on the different contact scenarios described in Section I-D and divided into four control modes. Depending on the mode, a velocity controller or force controller with corresponding constraint parameters is activated. The control strategy is tested in experiments that includes the three situations from Section I-D. The obtained test results are evaluated and the behavior discussed.

### A. Ropod and controller parameters

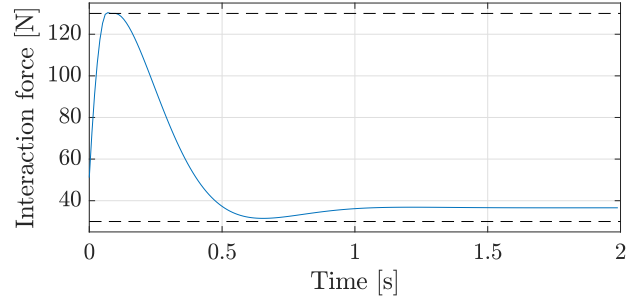
In order to simulate and implement Z-MPC on the ropod, the weight and viscous friction of the robot have to be determined. The weight of the robot has been measured by weighing the robot and is determined to be  $44kg$ . To determine the viscous friction of the robot, the required force is measured to move at a certain speed. A number of measurements have been carried out, in which the velocity controller makes the robot move at different speeds. The measurement is done from speeds of  $0.2m/s$  to  $1.6m/s$  with steps of  $0.2m/s$ . Speeds below  $0.2m/s$  are not taken into account because then strikeback friction also plays a role and we are now only interested in measuring the viscous friction. The viscous friction is assumed to be linear and so a first-order polynomial is fitted through the measurement data. This measurement is performed for both translation and rotation. The viscous friction of translation is  $3.82 \pm 0.86Ns/m$  with confidence bounds of 95%. The complete measurement is described in Appendix B-B.

The parameters of the ropod platform, bumper system and controller are summed in Table I

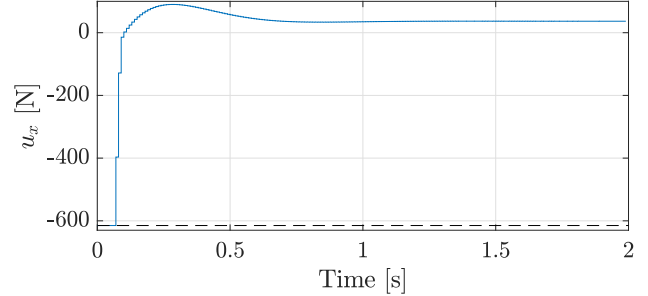
TABLE I: Controller and ropod parameters

Controller parameters:			
Sampling time sensors and Z-MPC	$T_s$	0.01	s
Weighting on input	$R$	1	-
Weighting soft constraints	$\rho$	$Ru_{max}^2$	-
Prediction horizon	$N$	20	-
Ropod parameters:			
Stiffness x bumper	$k_c$	2068	N/m
Damping x bumper	$b_c$	36.6	Ns/m
Stiffness y bumper	$k_c$	4489	N/m
Damping y bumper	$b_c$	36.6	Ns/m
Viscous friction translation robot	$b_r$	3.82	Ns/m
Mass robot mass	$M_r$	44	kg

The model used for Z-MPC is discretized with the Zero-order hold method and a sample time of  $T_S = 0.01s$ . This sample time corresponds to the fastest sample time possible with the sensors in the bumper. The prediction horizon of  $N = 20$  is chosen. With the sample time of  $0.01sec$ , this is a prediction of  $0.2s$ . This choice is based on the worst case scenario, a collision with an object. Without any control action, the interaction force stays below the upper constraint for speeds below  $0.47m/s$ . With this velocity, it takes  $0.2sec$  to reach the upper constraint. Therefore, with a prediction horizon of  $0.2sec$ , it can be predicted if the upper constraint is exceeded and if any control action is required. Also when we look at the frequency response of the system, the natural frequency of the systems lies at  $1.09Hz$ . When looking to the interaction force at collision of an uncontrolled system, the system oscillate with this frequency. Because of the damping and the initial speed, there is an interaction force at point of impact as shown in Equation (2). This courses a phase shift in the force signal. The time from impact to the first peak is therefore reduced to  $0.2sec$ . The required prediction horizon to detect this peak correspondents with this.



(a) Simulation of the interaction force. After collision a interaction force of 30N should be hold.



(b) Simulation of Z-MPC output.

Figure 14: Simulation of Z-MPC: collision with an object at maximal allowed initial speed.

### B. Z-MPC simulations

To initially test the control strategy of Chapter III, Z-MPC is simulated. The simulation is based on the situation where the robot has to make contact with an object without violating the maximal allowed interaction force and afterwards holds contact with that object. The parameters of Table I and II are used for this. The interaction will happen with the fond side of the robot, and maximal motor power is available to maintain the interaction force within bounds.

TABLE II: Constraints Simulation

Minimal deflection bumper	$x_l^{low}$	0.000	m
Maximal deflection bumper	$x_l^{high}$	0.070	m
Minimal motor power	$F_{rx}^{low}$	-615	N
Maximal motor power	$F_{rx}^{high}$	615	N
Minimal interaction force	$F_{dx}^{low}$	30	N
Maximal interaction force	$F_{dx}^{high}$	130	N

In Figure 14a the interaction force is shown. The initial speed of this experiment was  $1.4m/s$ . The force stays below the maximal bound and afterwards holds the interaction force above the lower bound. In Figure 14b the control action is shown. Z-MPC predicts that the maximum negative output force is required to break and hold the interaction force within bounds. Afterwards, a positive force is required to hold the robot connected to the object. When looking to the frequency response of the system, we can see a resonance peak at  $1.09Hz$  as described in Section IV-A. With a prediction horizon of

0.2sec, MPC can predict less than 1/4 of the oscillation. This prediction is too short to estimate that the system converges to the lower bound. Therefore MPC generates a output higher than 30N which holds the force a above the lower bound. This effect has also a benefit when the measurement data contains noise. Small perturbations in the force signal as a result of noise, will not result in exceeding the lower bound. The offset can be removed by increasing the prediction horizon, but this will cost more computation power.

### C. Implementing the controller on the ropod platform

1) *Signal processing:* When doing an experiment on the ropod platform, the interaction force is measured indirectly with distance sensors. A distinction is made between forces from x- and y-direction and the toque  $\theta$ . The measured forces are oriented in the opposite direction as the coordinate system of the ropod as shown in Figure 15. Interaction forces on the bumper are measured in four places on each side. Forces in the same direction are added together:

$$F_{dx} = F_{dx1} + F_{dx2} + F_{dx3} + F_{dx4} - F_{dx5} - F_{dx6} - F_{dx7} - F_{dx8} \quad (31)$$

$$F_{dy} = F_{dy1} + F_{dy2} + F_{dy3} + F_{dy4} - F_{dy5} - F_{dy6} - F_{dy7} - F_{dy8} \quad (32)$$

This way the robot can deal with multiple forces from different directions and the robot does not respond when these forces cancel each other out.

Z-MPC uses sensor data to calculate the required control output to keep the system within the constraints. The sensor data contains noise that can be seen in the output of the controller and can result in unnecessary control actions. To minimize the noise of the measured signal, a filter is added. For the choice of the filter, we looked at the frequency response of the system. Without control action, the system oscillates with a natural frequency of 1.09Hz. Signals with frequencies above the 1.09Hz can therefore be ignored. Also we have looked at the frequency response of the unfiltered sensor signal from a experiment with a collision with an object. This analyse is worked out in Appendix B-D. When looking at the cumulative power of the frequencies, we can see a strong increase until 5Hz as a result from the oscillating system at point of impact. Above the 5Hz, a much lower slope is visible as a result of noise. To filter the signal, we use a first order low-pass filter with a cut-off frequency of 5Hz. With this frequency, we have a balance between on one hand a low enough frequency to get a useful signal and on the other hand only a phase lag of 12° at 1.09Hz.

To measure the deflection of the bumper as a result of interaction forces, the measured interaction force is calibrated and set to zero each time the program is started. After the bumper is used for some time, the measured interaction force sometimes

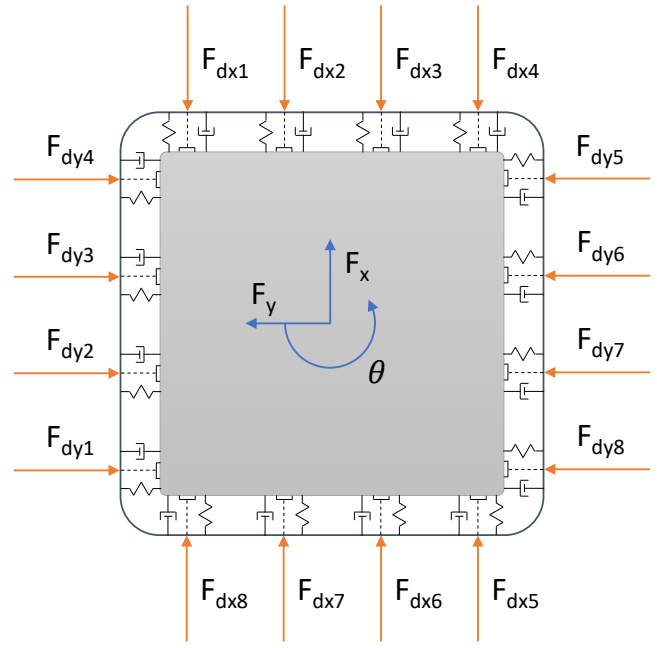


Figure 15: Schematic representation of the bumper system mounted on the ropod. The bumper is discretized into four parts at every side of the robot. Those parts have there own theoretical spring, theoretical damper and distance sensor. This way four forces are measured at every side of the bumper.

shows drift caused by temperature or voltage differences [21]. To deal with this drift, a high-pass filter is added. This filter has a cut-off frequency of 0.03Hz. This frequency is high enough to deal with the drifting but also low enough so the phase lag is only 1° at 1.5Hz. The high-pass filter can only be applied to the y-signal. This because in the x-direction, the situation can occur where the bumper is compressed for a long time when for example the robot is docking to a cart. With a high-pass filter, the filtered signal will then become zero over time. The calculated force in the x-direction is less affected by the drifting of the distance measurement because the stiffness is lower so the drifting is less amplified. Therefore the drift will not be a problem for short time experiments. But when the robot is used for a long time, this can cause problems.

2) *Modes of operation:* The control strategy is built up of different layers. High layers have information about the robot's handling in the hospital. Those determine the actions of the robot and thus the movements of the robot in the form of velocity commands. These velocity commands are sent to the low-level controller which ensures that the robot moves at the desired speed and in the desired direction. When the robot has to deal with interaction forces via the end-effector, the force controller will dominate the velocity controller to ensure a safe situation. The system is then switched to a different mode. The higher control layers have more information about the situation and can determine whether it is safe to continue in the normal operation mode or if other actions are required. If it is safe to



TABLE III: Constraints

Minimal deflection x bumper	$x_1^{low}$	0.000	$m$
Maximal deflection x bumper	$x_1^{high}$	0.070	$m$
Minimal deflection y bumper	$y_1^{low}$	0.000	$m$
Maximal deflection y bumper	$y_1^{high}$	0.035	$m$
Mode 2, collision with object:			
Minimal motor power x	$F_{rx}^{low}$	-212	$N$
Maximal motor power x	$F_{rx}^{high}$	212	$N$
Minimal interaction force x	$F_{dx}^{low}$	-130	$N$
Maximal interaction force x	$F_{dx}^{high}$	-20	$N$
Mode 3, interaction force from side:			
Minimal motor power y	$F_{ry}^{low}$	-100	$N$
Maximal motor power y	$F_{ry}^{high}$	100	$N$
Minimal interaction force y	$F_{dy}^{low}$	-70	$N$
Maximal interaction force y	$F_{dy}^{high}$	70	$N$
Mode 4, connect to cart / wall:			
Minimal motor power x	$F_{rx}^{low}$	-212	$N$
Maximal motor power x	$F_{rx}^{high}$	212	$N$
Minimal interaction force x	$F_{dx}^{low}$	20	$N$
Maximal interaction force x	$F_{dx}^{high}$	130	$N$

continue, the normal operation mode will be activated again and the robot can continue its way. To react as required on the different situations described in Section I-D, the robot skill has 5 operation modes:

- 1) Mode 0: Velocity control mode
  - Velocity control in all directions
  - Interaction forces are not taken into account
- 2) Mode 1: Normal operation mode
  - Velocity control in all directions
- 3) Mode 2: Collision with an object
  - Force control x- and y-direction
- 4) Mode 3: Interaction force y-direction
  - Force control y-direction
  - Velocity control x-direction
- 5) Mode 4: Connect to cart / wall
  - Force control x-direction and rotation

Mode 0 is used in the case when the robot is restarted and the sensors of the bumper are recalibrating or in the case the robot is in an unknown state and reactions from the force controller are unwanted. Normally the robot will function in mode 1 where the velocity controller is activated. When interaction forces are measured higher than a minimal bound, the system will switch to mode 2 or 3 to react on them. When the interaction forces are again below the lower bound, the system goes back to the normal operation mode. To prevent switching mode when the force is around the bound, a hysteresis element is added. Mode 4 is activated when the robot moves backward to connect to a cart or a wall. In the case a cart is connected to the robot, forces from the back of the robot are ignored by the force controller in mode 2 and 3. Those forces are still measured so they can be used by a higher control level to ensure the cart is still connected or if there is a collision with the cart when the robot is moving backwards.

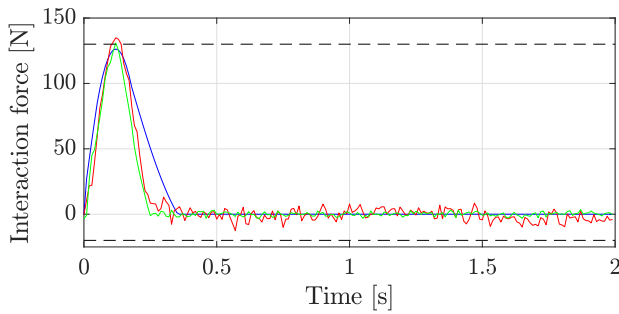
3) *Velocity control*: In situations where the robot is in velocity control mode, the robot is functioning using the existing platform velocity controllers. The velocity controllers are split up in x, y, and rotational direction and can be activated separately. The velocity controllers get a velocity setpoint from the navigation control layer so the robot can maneuver autonomously in the hospital.

4) *Force control*: When the interaction forces are measured, the velocity controller will be overruled by the force controller that can handle the interaction forces. The designed Z-MPC can be used for different situations by simply changing the parameters. Z-MPC is implemented on the ropod for x- and y-directed forces. The corresponding stiffness and damping parameters of the bumper are used in those controllers. To let the controllers react differently in different situations, the constraints are also adjusted to the mode. In Table III the different constraints for the different modes are described. In the case of a collision, full motor power is required to come to a standstill and the maximal allowed interaction force is set as upper constraint. In the case of sideways interaction forces, the motor power is limited to  $70N$  so the ropod will not react too aggressively. This can be done because the robot is not expected to move actively sideways and so strong collisions in y-direction are assumed not to occur. The constraints on the maximum allowed interaction forces have also been reduced so that the ropod respond more actively to interaction forces. The upper constraint will be reached with lower interaction forces so the robot has to react earlier / harder to prevent this. These parameters can be easily be adjusted to suit the wishes of the user. At last, we have the situation of the docking with a cart. Here also a minimal interaction force is added to hold contact with the object. The maximal interaction force can be reduced to prevent damage to the cart.

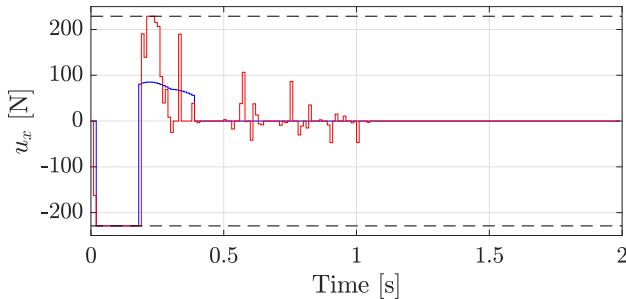
#### D. Experiments results

Three situations are tested with the ropod platform: collision with an object, connect to cart and interaction force from the side while the robot is navigating. For those experiments, the parameters of Table I and Table III are used.

1) *Experiment: collision with an object*: In the first experiment, a collision with an object (mode 2) is tested. A video of such an experiment can be seen with this link. The robot speed is slowly increased until it was not any longer possible to hold the maximal interaction force below the safe bound of  $130N$ . This could be done until a speed of  $0.7m/s$ . A higher speed will result in violating the maximal bound as shown with the red line in Figure 16a of an experiment with a speed of  $0.74m/s$ . Z-MPC predicts that with this speed, the interaction force will become too high and therefore the maximum allowable breaking power is used to prevent this as shown in with the red line in Figure 16b. Because of the lower detection threshold of  $20N$  before Z-MPC is enabled and the low-pass filter, there is a delay of  $0.01sec$  before the controller reacts on the interaction force. After breaking, a



(a) The interaction force at collision with an initial speed of  $0.74m/s$ . The red line is the interaction force of an experiment, measured by the bumper. The blue line is the simulated interaction force from the model that is used for MPC. The green line is the interaction force of that same experiment only than measured by a force sensor. The dotted lines are the force constraints.



(b) The controller output at collision with an initial speed of  $0.74m/s$ . The red line is the control action from the controller in the experiment. The dotted lines are the force constraints. Due to slip and a limited current, the constraints are at  $\pm 229N$ . There is a delay of  $0.01sec$  before the controller reacts because of the threshold that activates MPC and a delay in the input from the low-pass filter. There is also a delay in the output from the amplifier. The blue line is the simulated control action from MPC, including the limited braking power and delay in input and output.

Figure 16: Experiment: collision with an object.

forward force is generated to prevent the predicted force will become below the lower bound. This prevent a kickback from the system and oscillating behaviour. The maximal reached speed in the experiments is lower than the theoretical possible speed of  $1.4m/s$ . This is caused by multiple reasons. The main reason is that the maximal current of the wheels is limited to  $10A$  per wheel, multiplying this by the eight wheels and the current to force constant of  $2.86N/A$ , calculated in Appendix B-C, comes to a total braking power of  $229N$  that is possible to generate. This is lower than the  $615N$  which was defined in Section II-A. Increasing this current limit resulted in hardware problems as rebooting of the smart wheels, and is therefore not possible with the current setup. Also the wheels will have problems breaking with a higher current, due to slip. Another reason why it was not possible to maintain a safe interaction force above  $0.74m/s$ , is that it costs some time before the required force is generated by the wheels. In the static experiment of Appendix B-C, it took  $0.03sec$  between the moment the maximal current was set by the controller, and

the moment the corresponding force of  $229N$  was measured by the force sensor. This can be caused by the amplifier and/or dynamic behaviour of the system. This delay was not taken into account in the bumper design. The experiences from this experiment should be taken into account when designing the final end-effector, for a speed of  $1.4m/s$ .

The blue line of Figure 16 shows the simulated version of this experiment, with a initial speed of  $0.74m/s$ , a limited force output of  $229N$  and a delay from the lower detection threshold and low pass filter of  $0.01sec$  and the delay of  $0.03sec$  from the amplifier. The resulting behaviour of the controller in simulation is similar as in the real experiment, in which the maximal of  $229N$  braking power is used to try to hold the interaction force below the upper bound.

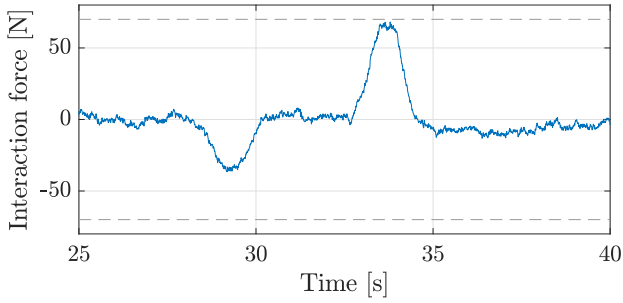
To verify that the interaction force measured by the bumper is corresponding with the real interaction force, a force sensor is placed in front of the bumper. The measurement data of this sensor is shown as the green line in Figure 16a. The peak of this line lies on the maximal bound of  $130N$  and indicates a safe interaction force. The force measured by the bumper is slightly higher than the real one which indicates an overestimation of the stiffness of the bumper. The overestimation of the stiffness is a result of using the mean stiffness measured over the complete bumper, while in reality the stiffness in the corner of the bumper is higher than the one in the middle. The real interaction force at the middle of the bumper will therefore be lower than the measured one, which can result in the controller reacting more aggressively than necessary. Despite the fact that the bumper is made of relatively cheap materials, cheap sensors are used and the stiffness is not exactly the same everywhere at the bumper, this bumper design can still be used. Z-MPC will use the available constrained output to keep the interaction force within limits.

### 2) Experiment: multiple interaction forces from the side:

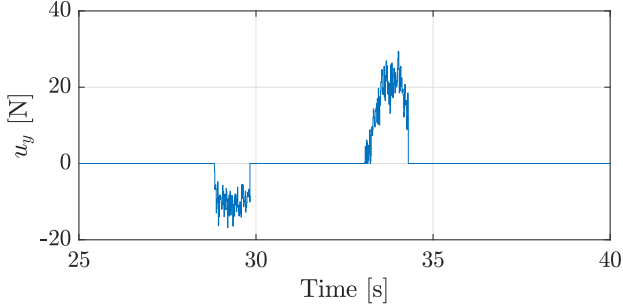
Figure 17 shows the second experiment, where the ropod is moving with a constant speed in a forward direction and forces are pushed against the bumper at the side (mode 3). A video of this experiment can be seen with this link. The controller reacts actively by moving the ropod in the desired direction. Because the outputs of the motor are limited at  $100N$  the ropod will not react too aggressively. When the connection is lost, the velocity controller in the y-direction is activated again and the ropod will continue to follow the reference.

### 3) Experiment: connect to a cart:

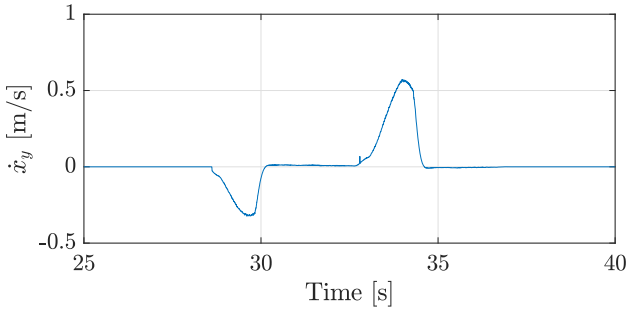
Figure 18 shows the third experiment, where the ropod is docking to a cart (mode 4). A video of this experiment can be seen with this link. Here we have a minimal interaction force constraint so contact with the cart will not be lost. First, the ropod moves to the card and tries to align in front of the cart. The ropod moves at a slow speed, in this case  $0.3m/s$ , backward to the cart. After making contact with the cart, Z-MPC is enabled and predicts that active braking is not necessary and therefore the control action is zero in the beginning. To hold contact with the cart, a minimal bound is set to  $-20N$ . When the controller predicts



(a) The interaction force measured on the sides of bumper. The dotted lines indicates the force constraints. This interaction force has to be kept within those constraints.



(b) The controller output that tries to keep the interaction force within constraints.



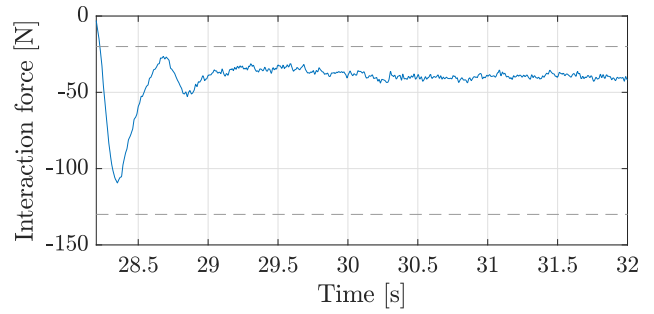
(c) The speed of the ropod in y-direction. The compliant control moves the ropod actively in the desired direction.

Figure 17: Experiment: sideways interaction force.

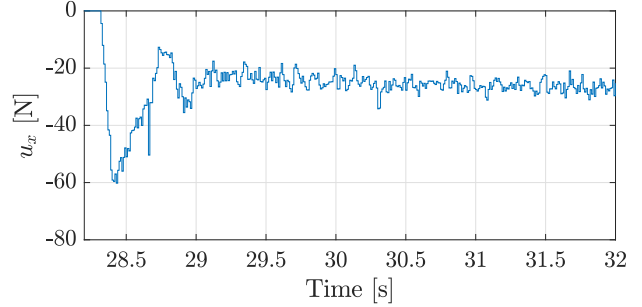
that the interaction force with the cart will be lost, a force is generated, pushing the robot against the cart. Also a PD torque controller is activated that tries to get the torque, measured by the bumper, to zero. This way the ropod also aligns parallel with the cart. After the cart has been coupled to the ropod, the ropod can move away with the cart. Forces generated by the cart against the back of the bumper are measured but ignored by the controller after coupling.

## V. CONCLUSIONS AND FUTURE WORK

To provide safety when a mobile robot is moving in an environment shared with people, we have designed a cost-effective passive compliant end-effector, as well as a compliant control strategy and implemented this on the ropod platform.



(a) The interaction force measured by the bumper. The dotted lines indicates the force constraints. The After making contact with the cart, a force is generated so connection with the cart will not be lost.



(b) The controller output. The controller predicts that a force of around 20N is required to hold contact with the cart.

Figure 18: Experiment: dock to cart.

As an end-effector a bumper is designed out of low-priced materials like standard aluminium profiles, rubber and standard available distance sensors. Z-MPC is chosen as compliant controller because of the possibility to handle constraints, predict future states and therefore the possibility to prevent violating the force constraints. With the zone addition, the controller reacts only when necessary to hold the force within constraints and otherwise let the passive bumper handle the interaction force. Initial validation was made via simulations. Afterwards, the bumper is built and the compliant control strategy tested experimentally. We noted that the bumper has a stiffness variation from  $2068N/m$  in the middle part which increases to  $3925N/m$  at the ends. Additionally, we found that the maximal breaking power was lower in practice due to hardware limitations and loss of grip in the wheels. There is also a delay in the input of the controller from the low-pass filter and on the output from the amplifier. The experiment was therefore tested at a maximum speed of  $0.74m/s$ . Due to the stiffness variations and an overestimated equivalent stiffness, the real interaction force was lower than the measured one by the bumper. Despite this, the results showed that the controller was able to hold the interaction force within the limits by predicting the force violation and reacting on forehand with maximal allowed breaking power. The compliance behaviour of the controller is tested in the case of multiple interaction forces from the side of the bumper, in which the ropod moves actively in the direction of the force. The robot is also able to

dock to a cart and hold a minimal interaction force with it.

For future work we can make the following possible improvements:

- 1) Because of the way the rubber bumper is designed, it contains a variation in the stiffness. This results in an overestimated interaction force in the middle part of the bumper. To remove this mismatch, change the bumper design to get a more uniform stiffness. Another possibility is to include those differences in the measurement by connecting the different stiffness it to the corresponding sensor. To be able to realize this, the model used for MPC gets more inputs. The drawback of this solution is that the prediction model becomes more complicated and this can result in a higher computation time when calculating the output of the controller.
- 2) The interaction force is calculated from distance sensor measurements. Those measurements contain noise that can be seen in the calculated force. In the case the ropod is connected to a cart, the interaction force is held close to the lower bound. The noise can make the force measurement violate the lower constraint as in reality this is not the case. When the force constraint is violated, the controller will try to get the system within bounds as fast as possible. This results in undesired control action. This can be solved simply by adding a constant force to the output of the controller after making contact with the cart. But this solution will create a mismatch in the prediction model of MPC and will not adapt to variations in the interaction force, when, for example, this force becomes too high. Because of those drawbacks, an other solution like for instance incorporating the minimum contact force in the cost function could solve this problem in a more controlled way.
- 3) The deflection measurements show drift after some time. To compensate for this, a high-pass filter is applied. This can only be done on the y-signal because in x-direction, the situation can occur where the bumper is compressed for a long time when for example the robot is docking to a cart. With a high-pass filter, the filtered signal will become zero over time. When the robot is used for a long time, this can cause problems. A possible solution is to add the high pass filter when the robot is in normal operation mode and deactivate this filter when the ropod has to connect to a cart.
- 4) A safe collision with the speed of  $1.4m/s$  was not possible. This problem has multiple causes. It was not possible to break with  $615N$  but only with  $229N$  due to the current limiter and slip of the wheels. The current was limited to  $10A$  otherwise the smartwheels rebooted in case of hard breaking. The hardware has to be examined to exactly establish where this behaviour comes from. When a higher current is possible, the slipping of the wheels will increase. This slip can be reduced with for example other type of rubber on the

wheels. It takes also some time between the moment the current is set to the wheels and the corresponding force is generated. If it is possible to remove this delay of  $0.03sec$ , a speed of  $0.9m/s$  should already be possible.

- 5) The low level force controller of the ropod platform can be improved. When the robot is moving, the smart wheels can show oscillating behaviour. This is now solved by a velocity controller on wheel basis that is adding damping. Because this controller is interfering with the force controller, this controller is replaced, when the force controller is enabled, by a controller that adds damping to the smart wheel angle velocity. Also an active compensation is added to make the smart wheels turn in the desired direction when somebody pushed the ropod in a different direction. The angle velocity controller and flip compensation need to be worked out further and tested for higher speeds as well.

#### ACKNOWLEDGEMENT

With this thesis, my learning experience at the CST research group from the TU/e comes to an end. During my graduation I met many interesting people who helped me with this project. I would like to thank a few people for making it all possible.

First of all, I would like to thank my direct coach, Cesar Lopez, who helped me in this project during our weekly meetings with the problems I faced. One of the most valuable lessons he taught me is to take a very critical look at the results of my measurements before drawing conclusions.

I would also like to thank my supervisors, René van de Molengraft and Herman Bruyninckx, who have taken a critical look at my work during our biweekly meetings, gave me advice and let me reconsider the choices I have made in this project to end with a deliberate end result.

Besides these people, I would also like to thank the ROPOD project for providing the ropod platform that I have used for the experiments and for making the construction of the bumper financially possible.

ROPOD is an Innovation Action funded by the European Commission under grant no. 731848 within the Horizon 2020 framework program.

#### REFERENCES

- [1] "Healthcare robotics." <https://cacm.acm.org/magazines/2017/11/222171-healthcare-robotics/fulltext>, September 2018.
- [2] "Robots help teach stem concepts to students with autism." <https://robohub.org/uav-based-crop-and-weed-classification-for-future-farming/>, September 2018.
- [3] "Robots help teach stem concepts to students with autism." <https://www.roboticsbusinessreview.com/consumer/robots-help-teach-stem-to-students-with-autism/>, September 2018.
- [4] A. B. M. Vasic, *Safety Issues in Human-Robot Interactions*. International Conference on Robotics and Automation, 2013.

- [5] "Ropod — hochschule bonn-rhein-sieg (h-brs)." <https://www.h-brs.de/en/ropod>. (Accessed on 02/09/2018).
- [6] M. Van Damme, P. Beyl, B. Vanderborght, R. van Ham, I. van der Niepen, A. Matthys, P. Cherelle, and D. Lefeber, *The Role of Compliance in Robot Safety*. Vrije Universiteit Brussel, 2010.
- [7] M. Al Abbassi, *Dynamical Wall-Following for an Autonomous Mobile Robot*, CST 2017.087. Eindhoven University of Technology, 2017.
- [8] E. Mitka, A. Gasteratos, N. Kyriakoulis, and S. G. Mouroutsos, *Safety certification requirements for domestic robots*. School of Engineering, Democritus University of Thrace, 2012.
- [9] S. Oberer-Treitz, T. Dietz, and A. Veri, *Safety in industrial applications: From fixed fences to direct interaction*. Fraunhofer Institute for Manufacturing Engineering and Automation IPA, 2013.
- [10] G. F. L. Bascetta, E. D. P. Rocco H. Ardo H. Bruyninckx, and E. D. Lello, *Towards safe human-robot interaction in robotic cells: an approach based on visual tracking and intention estimation*. IEEE/RSJ, 2011.
- [11] D. Althoff, J. Kuffner, D. Wollherr, and M. Buss, *Safety assessment of robot trajectories for navigation in uncertain and dynamic environments*. Springer Science+Business Media, 2012.
- [12] S. Haddadin, A. Albu-Schffer, and G. Hirzinger, *Requirements for Safe Robots: Measurements, Analysis and New Insights*. The International Journal of Robotics Research, 2009.
- [13] S. Norouzzadeh, T. Lorenz, and S. Hirche, *Towards Safe Physical Human-Robot Interaction: an Online Optimal Control Scheme*. International Symposium on Robot and Human Interactive Communication, 2012.
- [14] N. Tagliamonte, F. Sergi, D. Accoto, G. Carpino, and E. Guglielmelli, *Double actuation architectures for rendering variable impedance in compliant robots: A review*. Center of Integrated Research, Universit Campus Bio-Medico di Roma, 2012.
- [15] D. Rus and M. Tolley, *Design, fabrication and control of soft robots*. Macmillan, 2015.
- [16] A. E.-N. G.F. Franklin, J.D. Powell, *Feedback Control of Dynamic Systems*. Pearson Education Limited, 2014.
- [17] M. U. A. S. S. U. Farooq, K.M. Hasan, *Fuzzy Logic Based Wall Tracking Controller for Mobile Robot Navigation*. University of The Punjab Lahore-54590 Pakistan, 2012.
- [18] A. M. C.E. Garcia, *Quadratic Programming Solution of Dynamic Matrix Control*. Shell Development Company, 1985.
- [19] V. Utkin, *Sliding Mode Control*. The Ohio State University, Columbus, Ohio, USA, 2009.
- [20] J. Maciejowski, *Predictive Control with Constraints*. Pearson Education, 2000.
- [21] STMicroelectronics, *Proximity and ambient light sensing (ALS) module*, March 2016. Rev. 7.

## APPENDICES

### APPENDIX A BUMPER DESIGN

To be able to make the ropod platform safe to use, a prototype of an end-effector is designed and built. All contact between the moving robot and an object will occur through this end-effector. The designed end-effector should be cost-effective, corresponding to the goal of the ropod project. It should also have sufficient stiffness and damping to be able to handle force interactions. To satisfy those requirements, a rubber

bumper is chosen as a design for this prototype, made of standard available rubber and profiles. These profiles are made of aluminium to prevent corrosion, be lightweight and to match the ropod. The rubber bumper system creates a passive compliant design that is required in the context of robotic interaction. Because it is made of soft material, it provides the safety for both the robot and the environment. A disadvantage of a rubber bumper is that the stiffness is not exactly linear and also not equal at every location. Despite these deviations, it is still possible to use this design because of the robustness of the force controller. Using this bumper for experimental purpose will point out further improvements that can be used to design the final end-effector.

The bumper is made out of four corner parts that are connected together for a stiffer connection. Four corner pieces were chosen so the connection point is not at the corner but in the middle and it is easy to handle and install on the ropod platform. The aluminium profile has been cut and set at 90° Figure 19-(1). This way a stiff corner piece is obtained which consists of one piece. The loose parts are connected to each other at the rear with a connecting plate Figure 19-(2) that provides extra strength. The rubber is clamped between the angular-profile and the u-profile Figure 19-(3). At the bottom of the u-profile the rubber is clamped with the help of allen screws. To prevent tearing of the rubber, the surface of the allen screws is increased by the use of plain washer. These are placed at equal distance from each other to keep the rubber as flat as possible. Corners are created by cutting the rubber at the fold to be able to bend the excess rubber away Figure 19-(4). The end of the cuts are drilled to prevent tear. An obtuse angle of the rubber has been chosen in order to be able to

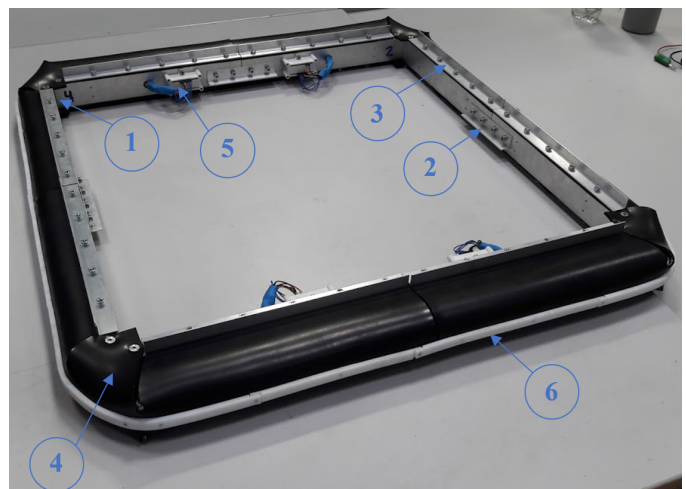


Figure 19: Prototype of bumper system for ropod platform. build from four bended corner parts (1). connected with connection strip (2). The rubber is clamped by aluminium profile(3). Corners are made by cutting and folding the rubber (4). Arduino is placed on the inside of the bumper (5). A nylon strip is placed around the bumper (6).



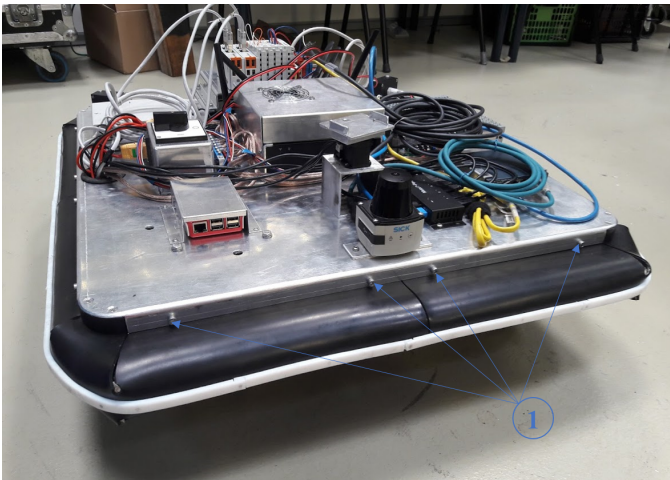


Figure 20: Bumper system mounted on ropod platform. The bumper system can be installed easily by the screws in the edge (1).

accommodate to small variations such as a hinge when the robot is sliding along a wall. Because the corners are folded, here the stiffness is higher than at middle part of the bumper. This should be taken into account in the controller design.

The width of the robot is limited. In order to make maximum use of the space, the bumper is mounted under the edge of the robot. The part of the bumper which protrudes from under the robot is therefore also the area that can be compressed. To attach the bumper under the robot, the angular-profile Figure 19-(3) is used to connect the bumper to the edge of the robot. The fastening screws of the bumper are therefore easily accessible Figure 20-(1).

Force measurements are required to control the robots movement, this way it is possible to measure if the interaction force stays between safe bounds. The force measurement is done indirectly by measuring the deformation of the rubber. With an estimation of the stiffness and damping of the rubber, it is possible to calculate the interaction force. The VL6080X time of flight short range distance sensors are placed at the back of the u-profile. 16 sensors are evenly distributed with a spacing of  $164\text{mm}$  around the bumper. The VL6180X contains a tiny laser and matching sensor that can detect the time of flight, or how long the laser light has taken to bounce back to from the inside of the bumper to the sensor. The sensor can handle about  $5\text{mm}$  to  $100\text{mm}$  of range distance. Because the sensor is placed in the u-profile, the maximal compression of the bumper falls well within the measuring range of the sensor. Communicating to the sensor is done over I2C bus. The sensors are started one by one after which a unique address is given to the sensor. This way it is possible to read multiple sensors that are connected to the same I2C bus. The distance sensors are read out with an Arduino. Every corner part has its own Arduino Figure 19-(5) that is connected to the PC of the robot trough USB. A so called 's-function' is made that

contains c-code to communicate with the Arduino over serial connection. This s-function can be used in MATLAB Simulink to access the sensor data and use this for controlling the ropod. The bumper is modelled as four springs and dampers, discretized over the four distance sensors at each side of the bumper. This way the force acting at four parts of the bumper is measured. In order to measure deformation at a point between two sensors, a nylon strip Figure 19-(6) is paced around the outside of the bumper. This relative stiff strip will help to distribute the interaction force evenly over the bumper. It also reduces the friction force between the rubber bumper and an object when the robot sliding along one. The location of the interaction force with respect to the centre of the robot is also taken into account. This way the torque applied on the robot can be calculated, which can be used to align with a cart.

## APPENDIX B PARAMETER MEASUREMENT

To be able to implement Z-MPC, the parameters of the system need to be determined. Those parameters are used in for example in the prediction model and for designing the filters. In this appendix the measurement are described in more detail.

### A. Stiffness measurement

Hooke's law of equation (4) is used to determine the stiffness. A load cell is pressed against the bumper and the interaction force with the associated deformation is recorded. A graph can be made of the force against the deformation. The stiffness of the bumper is considered to be linear so a first order polynomial can be fitted through the measurement data. The stiffness of the bumper is equal to the slope of the polynomial. This measurement is performed for the prototype of the end-effector and the results are shown in the graph of Figure 21. The stiffness of the bumper with a thickness of  $35\text{mm}$  is  $4489\text{N/m} \pm 132\text{N/m}$  with 95% confidence bounds and the one with thickness of  $70\text{mm}$  is  $1513\text{N/m} \pm 24\text{N/m}$  with 95% confidence bounds.

When the ropod has a collision with a big object or has to connect to a cart, not a small area but the complete bumper is compressed. Those situations mainly happen in the front and back of the ropod with the  $70\text{mm}$  thick bumper. Because the stiffness in the corner of the bumper is higher than in the middle, this can create a offset in the measure interaction force and the real force. Extra measurements are done to determine the stiffness variation of those parts of the bumper. The stiffness of the complete bumper is determined in an experiment where the full length is compressed. The measured stiffness in that experiment is  $8275\text{N/m} \pm 359\text{N/m}$  with 95% confidence bounds. So the sections in the middle of the bumper have a stiffness of  $1513\text{N/m}$  and this increases at de edges to become a total of  $8275\text{N/m}$ . To determine exactly where the areas lie that have a higher stiffness, a force sensor is moved

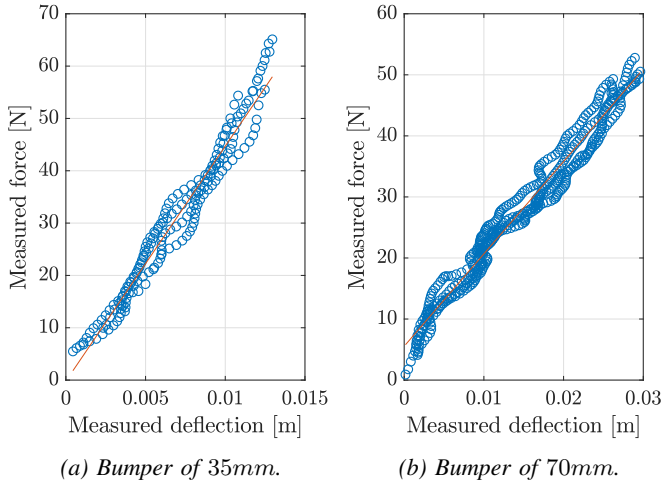


Figure 21: Stiffness measurement.

along the bumper while compressing it with a fixed distance. At the corner a stiffness of  $3925N/m$  is measured decreasing linear over a length of  $108mm$  to settle at  $1513N/m$  in the middle part. When moving further the stiffness stays the same, until it reaches  $108mm$  before the end of the bumper, where the stiffness is again increasing until  $3925N/m$ . When combining those measurement, the graph of Figure 9 can be made. The model used by the controller can only handle one stiffness so therefore the mean stiffness is used, calculated by dividing  $8275N/m$  over the four sensors, which comes out at a stiffness of  $2068N/m$  per sensor.

### B. Viscous friction ropod

To determine the viscous friction of the robot, it is important to measure which force is required to move the robot at a certain speed. A number of measurements have been carried out, in which the velocity controller let the robot move at different speeds. The speed at which the robot moves as well as the required force is measured. This measurement is repeated with a speed set points of  $0.2m/s$  to  $1.6m/s$  with steps of  $0.2m/s$ . Speeds below  $0.2m/s$  are not taken into account because then stribek friction also plays a role and we are only interested in the viscous friction. The maximal speed of the robot with the current controllers is  $1.6m/s$ . To verify the reliability of the outcome of the experiments, each speed-force measurement was performed tree times. When examine the results, we are interested in the time zone where the robot drives at a constant speed. The average of the forces in those areas has been calculated. The velocities are plotted against the forces in the graph of Figure 22. A line can be fitted through the measuring points where the slope of the line is equal to the viscose friction. The viscose friction of translation is  $3.82 \pm 0.86Ns/m$  with confidence bounds of 95%.

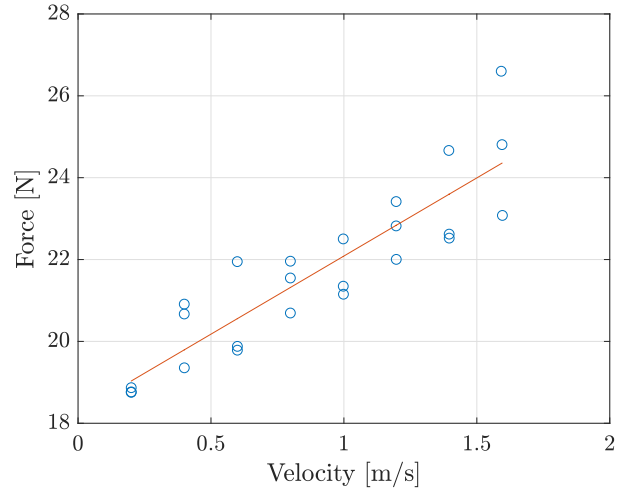


Figure 22: Friction measurement translation at different speeds. The Viscous friction is  $3.82 \pm 0.86Ns/m$  with 95% confidence bounds.

### C. Force measurement ropod

To be able to know the fore that is generated by the smart wheels, the current force constant is determined. The measurement is done in static situation in which the smart wheels of the ropod get a current set point and generates forward fore that is measured with a force sensor. The outcome of this measurement is shown in Figure 23. For this experiment, the time section where the ropod is generating a constant force is used. The average measured current  $I_q$ , used by the smart wheels is plotted against the average measured force of that same time window. In this experiment the  $I_d$  is kept at zero by the wheel controller. For the current force constant, the slope of the line fitted trough the data points is used. This slope has a value of  $2.86N/A \pm 0.13N/A$  with 95% confidence bounds. Divided by the number of wheels and multiplied with the diameter of the wheels, comes out on a current to torque constant of  $0.0186Nm/A$  per wheel.

### D. FRF sensor signal

The sensor data of the bumper contains noise. To be able to distinguish the noise from the data of interest, the frequencies of desired signal need to be determined. Based on those frequencies, a filter can be designed that filters out most of the noise. One method that is used to determine frequencies of the system, is by examining the frequency response. An experiment is done in which the ropod with the bumper has a collision with an object. The frequency response is shown in Figure 24a. An amplitude increase of frequencies up to  $5Hz$  can be seen. After that  $5Hz$  the noise has a more constant amplitude. This is also confirmed when looking to the cumulative power in Figure 24b. The cumulative power has a steep slope up to  $5Hz$ . After  $5Hz$  the slope decreases to a lower constant for the other frequencies. A low pas filter



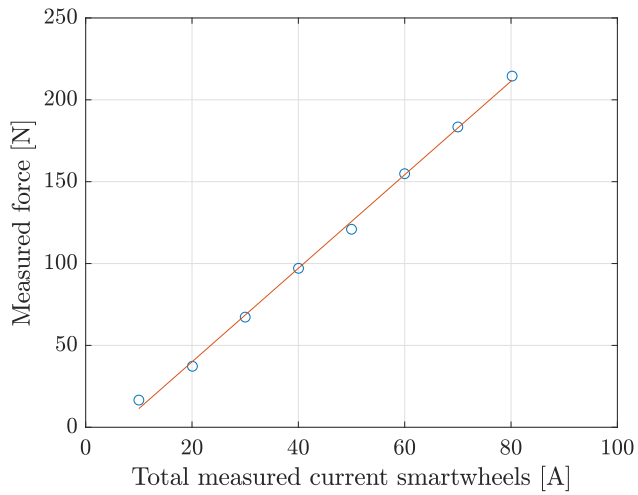
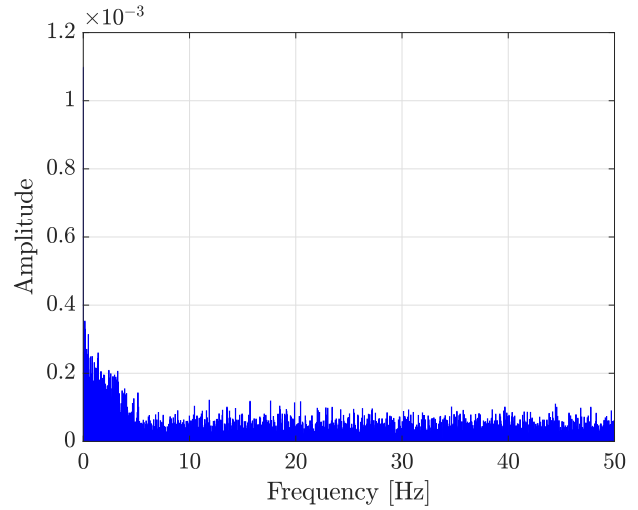
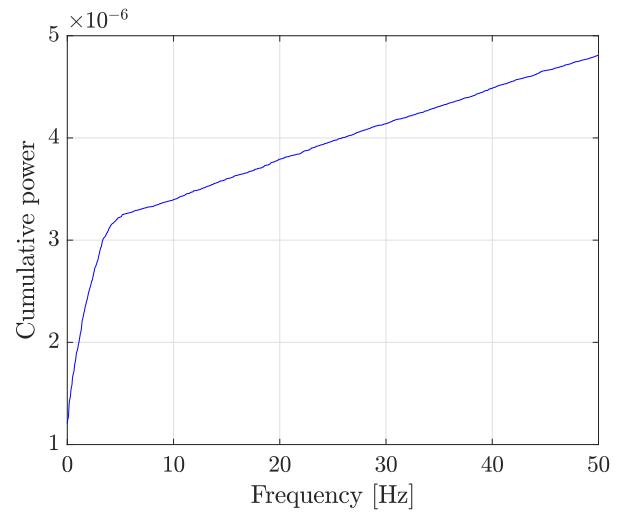


Figure 23: Measurement of current force constant. This constant is  $2.86N/A \pm 0.13N/A$  with 95% confidence bounds.

is designed on the basis of this measurement with a cut-off frequency of  $5Hz$ .



(a) Frequency response results of sensor data. The signal of inters is up to  $5Hz$  after that there is only noise.



(b) Cumulative power of the frequencies. The signal of inters is up to  $5Hz$  after that there is only noise.

Figure 24: Frequency response of measurement data of the bumper, in the case of a collision with an object.